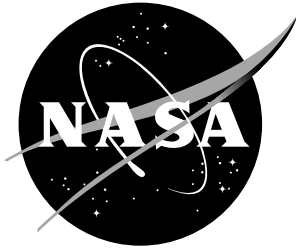


NASA/TM-2003-212420



Advanced Durability and Damage Tolerance Design and Analysis Methods for Composite Structures

*Lessons Learned From NASA Technology Development
Programs*

*Charles E. Harris, James H. Starnes, Jr., and Mark J. Stuart
Langley Research Center, Hampton, Virginia*

June 2003

The NASA STI Program Office . . . in Profile

Since its founding, NASA has been dedicated to the advancement of aeronautics and space science. The NASA Scientific and Technical Information (STI) Program Office plays a key part in helping NASA maintain this important role.

The NASA STI Program Office is operated by Langley Research Center, the lead center for NASA's scientific and technical information. The NASA STI Program Office provides access to the NASA STI Database, the largest collection of aeronautical and space science STI in the world. The Program Office is also NASA's institutional mechanism for disseminating the results of its research and development activities. These results are published by NASA in the NASA STI Report Series, which includes the following report types:

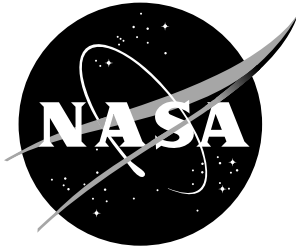
- TECHNICAL PUBLICATION. Reports of completed research or a major significant phase of research that present the results of NASA programs and include extensive data or theoretical analysis. Includes compilations of significant scientific and technical data and information deemed to be of continuing reference value. NASA counterpart of peer-reviewed formal professional papers, but having less stringent limitations on manuscript length and extent of graphic presentations.
- TECHNICAL MEMORANDUM. Scientific and technical findings that are preliminary or of specialized interest, e.g., quick release reports, working papers, and bibliographies that contain minimal annotation. Does not contain extensive analysis.
- CONTRACTOR REPORT. Scientific and technical findings by NASA-sponsored contractors and grantees.
- CONFERENCE PUBLICATION. Collected papers from scientific and technical conferences, symposia, seminars, or other meetings sponsored or co-sponsored by NASA.
- SPECIAL PUBLICATION. Scientific, technical, or historical information from NASA programs, projects, and missions, often concerned with subjects having substantial public interest.
- TECHNICAL TRANSLATION. English-language translations of foreign scientific and technical material pertinent to NASA's mission.

Specialized services that complement the STI Program Office's diverse offerings include creating custom thesauri, building customized databases, organizing and publishing research results ... even providing videos.

For more information about the NASA STI Program Office, see the following:

- Access the NASA STI Program Home Page at <http://www.sti.nasa.gov>
- E-mail your question via the Internet to help@sti.nasa.gov
- Fax your question to the NASA STI Help Desk at (301) 621-0134
- Phone the NASA STI Help Desk at (301) 621-0390
- Write to:
NASA STI Help Desk
NASA Center for AeroSpace Information
7121 Standard Drive
Hanover, MD 21076-1320

NASA/TM-2003-212420



Advanced Durability and Damage Tolerance Design and Analysis Methods for Composite Structures

*Lessons Learned From NASA Technology Development
Programs*

*Charles E. Harris, James H. Starnes, Jr., and Mark J. Stuart
Langley Research Center, Hampton, Virginia*

National Aeronautics and
Space Administration

Langley Research Center
Hampton, Virginia 23681-2199

June 2003

Available from:

NASA Center for AeroSpace Information (CASI)
7121 Standard Drive
Hanover, MD 21076-1320
(301) 621-0390

National Technical Information Service (NTIS)
5285 Port Royal Road
Springfield, VA 22161-2171
(703) 605-6000

**Advanced Durability and Damage Tolerance Design and Analysis Methods
for Composite Structures**
Lessons Learned from NASA Technology Development Programs

by

Charles E. Harris
James H. Starnes, Jr.
and
Mark J. Shuart
Structures and Materials Competency
Mail Stop 121
Langley Research Center
National Aeronautics and Space Administration
Hampton, VA 23681-2199

Abstract

Aerospace vehicles are designed to be durable and damage tolerant. Durability is largely an economic life-cycle design consideration whereas damage tolerance directly addresses the structural airworthiness (safety) of the vehicle. However, both durability and damage tolerance design methodologies must address the deleterious effects of changes in material properties and the initiation and growth of microstructural damage that may occur during the service lifetime of the vehicle. Durability and damage tolerance design and certification requirements are addressed for commercial transport aircraft and NASA manned spacecraft systems. The state-of-the-art in advanced design and analysis methods is illustrated by discussing the results of several recently completed NASA technology development programs. These programs include the NASA Advanced Subsonic Technology Program demonstrating technologies for large transport aircraft and the X-33 hypersonic test vehicle demonstrating technologies for a single-stage-to-orbit space launch vehicle.

Key Words

durability, damage tolerance, fatigue, fracture, structural integrity, structures, composite materials, graphite/epoxy, aerospace vehicles

Any use of company trademarks, trade names, or product names used herein does not indicate a NASA endorsement of those products.

Introduction

All aerospace vehicles must be designed to be durable and damage tolerant. This design imperative is dramatically illustrated in Figure 1. The fuselage failure of the Aloha Airlines Boeing-737 aircraft in 1988 and the uncontained engine failure of the Delta Airlines MD-88 aircraft in 1996 illustrate the need to design both durable and damage tolerant primary structure. Each failure was precipitated by the accumulation of undetectable fatigue damage. Durability is typically viewed as an economic life-cycle design consideration whereas damage tolerance is an attribute of the structure that is directly related to the vehicle safety. However, both durability and damage tolerance design methodologies must address the deleterious effects of changes in material properties and the initiation and growth of microstructural (undetectable) damage due to fatigue that may occur during the service lifetime of the vehicle. This requirement is particularly challenging to composite structural designers because composite materials are not isotropic (making damage growth prediction a complex process) and lack ductility (eliminating yielding as an indicator of imminent failure).

Composite structural design and manufacturing technology is not yet as mature as metallic structures for heavily loaded aerospace structural applications. The 65 years of successful experiences with the design of metallic structures cannot be directly transferred to the design of composite structures because the failure mechanisms for composite and metallic structures are different. There are several important factors that explain why composite structures fail differently than metallic structures. First, composite materials are not isotropic and homogenous like most aluminum alloys. Second, composite materials are generally brittle and lack the inherent benefit of the ductility exhibited by aluminum alloys. Third, the initiation and growth of material-level damage and the failure modes of composite structure are not as well understood and cannot be predicted accurately. Due to these complications, the current design and analysis methods are semi-empirical and rely heavily on the building-block approach to design and certification. In addition, the best design practices are only fully understood by those engineers who are experienced at designing composite structures.

Maintenance, inspection, and repair technologies for composite aerospace structures are also not yet as mature as for metallic structures for all applications. Many of the design and maintenance technologies to support metallic structures in everyday use today do not apply to composite structures. Furthermore, the long-term, field experiences necessary to develop a support infrastructure do not yet widely exist for composite structures. Therefore, support issues must be anticipated in the design phase for composite structures to help facilitate effective maintenance, inspection, and repair procedures. Structures must be designed so that they can be inspected and repaired in the field. In addition, nondestructive inspection experts should be part of the collaborative engineering design team so that inspectability is built into the structure from the outset of the design.

These added complexities in designing durable and damage tolerant composite structure are a primary barrier to expanding the application of composites to heavily loaded, primary structures. Accurate, reliable, and user-friendly computational methods, design optimization methods, and robust structural design concepts are currently under development to address the deficiencies of the current standard practices. In addition, more durable and damage-tolerant

material systems and manufacturing technologies are also under development for advanced aerospace vehicle applications. The current paper discusses the design and certification requirements for composite structure and the current industry standard practices. The status of advanced methods under development will be reviewed by presenting the results of two recently completed NASA technology development programs. These programs include the X-33 hypersonic test vehicle demonstrating technologies for a single-stage-to-orbit space launch vehicle, and the NASA Advanced Subsonic Technology Program demonstrating technologies for large transport aircraft wing structures.

Design and Certification Requirements

Aerospace structural components are designed to be very close to a zero design margin for design ultimate loads to avoid any unnecessary weight. The design limit loads are defined to be the highest loads that the structure is expected to experience at any time during its service history. Referring to Figure 2 [Ref. 1], the factor of safety between the design limit load and the design ultimate load is 1.5 for large transport, commercial aircraft [Refs. 2 and 3]. The Code of Federal Regulations [Ref. 2] for Aeronautics and Space, Title 14, specifies that the structure shall undergo no permanent deformation at the design limit load (DLL). In addition, the structure shall sustain the design ultimate load (DUL) for at least 3 seconds before failing. While the margin of safety is not equal to zero for all of the design criteria at each structural location, typically one criterion for each structural element governs the design details for that element. The quest for the lowest weight structure then drives the design margin to be nearly equal to zero for the design ultimate load condition. The factor of safety between the design limit load and the design ultimate load conditions often accounts for the difference between linear, elastic behavior and complete structural failure and for uncertainties in other parameters such as loads and material properties. Therefore, aerospace structural designs do not have a large design margin to accommodate any unanticipated deleterious structural behavior.

For large transport commercial aircraft [Refs. 2 and 3], “durability is defined to be the ability of the structure to retain adequate properties (strength, stiffness, and environmental resistance) throughout its service life to the extent that any deterioration can be controlled and repaired, if there is a need, by economically acceptable maintenance practices. Structural durability affects the frequency and cost of inspection, replacement, repair, or other maintenance. Damage tolerance is defined to be the ability of the structure to sustain design limit loads in the presence of damage caused by fatigue, corrosion, environmental effects, accidental events, and other sources until such damage is detected, through inspections or malfunctions, and repaired. Structural damage tolerance ensures that damage will be found by maintenance practices before becoming a safety threat.”

For manned spacecraft systems [Ref. 4], NASA defines a damage tolerant part as one that possessed the ability to resist failure due to the presence of cracks during its entire service life multiplied by the required service-life factor. “The service life factor for all NASA spaceflight hardware on manned systems is four (4). Damage tolerance evaluations shall be performed on all fracture critical parts to demonstrate their damage tolerance capabilities. (As used herein, fracture critical components are primary load path components where failure results in a loss of function and vehicle flightworthiness.) Damage tolerance evaluations shall be done by damage

tolerance analyses or tests. Evaluations shall assume that cracks exist in the most critical locations and orientations in the part based on flaw screening capability. For materials, such as composite materials, which may sustain hidden impact damage, the level of damage assumed in the evaluation shall be representative of the credible damage threat after inspection and prior to flight service. For components where neither damage tolerance, damage analysis, nor damage tolerance testing are appropriate, such as for some composite material failure modes, proof testing of each flight hardware item may be used to establish similar confidence in a part's damage tolerance."

The durability and damage tolerance design requirements cited above must also be addressed in conjunction with the design requirements for design limit load and design ultimate load. As shown in Figure 2, taken together, these requirements lead to definitions of the allowable damage limit and the critical damage threshold. The structure may have undetectable (allowable) damage provided that the design ultimate loads can be sustained. In contrast, the critical damage threshold defines the state of damage that must be detectable to ensure that the structure possesses adequate residual strength to sustain the design limit loads. Therefore, design requirements for composite structure are based on the concept that barely visible damage defines the critical damage threshold and also sets the design allowable values for design limit loads. Several examples of subcritical damage that may develop in composite structure are illustrated in Figures 3, 4, and 5. Matrix microcracking that commonly develops in many brittle epoxy systems is illustrated in Figure 3. Matrix microcracks often develop within the plies of a laminate at relatively low strain levels, especially in the off-axis 90° plies that are perpendicular to the principal loading direction. However, these ply-level cracks are usually inconsequential because they are constrained by fibers and cannot coalesce into a dominant crack that may lead to failure similar to fatigue crack growth in metallic structures. An example of a much more complex damage state is illustrated in Figure 4. This particular state of damage developed at a stress concentration (notch) when the structure was subjected to a tensile loading condition. The damage state consists of matrix cracks, fiber fractures, and delaminations. However, this highly complex damage state may not exceed the critical damage threshold for the structure. This observation is due to the beneficial strain-softening effect of the damage, which results in load redistribution away from the high stress-concentration region. Just like the crack growth resistance affect exhibited by ductile metals, the applied load must be increased for the damage state to grow beyond the critical damage threshold necessary to cause structural failure. Another type of damage in composites that may develop as a result of foreign object impact events is illustrated in Figure 5. Impact damage may be visible or undetectable (i.e., nonvisible) and may extend completely through the thickness of a laminate. Extensive test programs have illustrated the very large reduction in residual strength that may occur even in the case of undetectable impact damage [for examples, see Refs. 5-11]. This strength reduction is illustrated in Figure 6 where failure occurring when the impacted structures are subjected to compression loads is plotted as a function of impact damage severity [Ref. 11]. This damage state is particularly insidious because accidental impact events are a common occurrence. Therefore, the compression-after-impact test method to determine the sensitivity of a composite structure to low-speed impact damage has become an industry standard for developing the design allowable values used to meet the design limit load requirement.

The damage tolerance design approach that is generally used for many aerospace vehicles may be summarized as follows:

1. Determine the fracture critical components.
2. Determine the possible damage states that could exist in the component.
3. Determine the size of damage that could be missed (undetectable) by the initial manufacturing quality assurance inspection and by subsequent in-service inspections. This process sets the design allowable damage limit values.
4. Assume that the undetectable damage is present in each fracture critical component at the most critical location.
5. Determine the residual strength of the structure with undetectable damage that is required at the design limit load condition and the associated critical damage state.
6. Determine the extent to which the undetectable damage may grow during the service life of the vehicle and the point in life when the damage becomes critical for design limit loads. This process sets the critical damage threshold. The vehicle with critical damage must also survive a discrete source damage event such as an uncontained rotor burst.
7. Develop an in-service inspection program (method and inspection intervals) that will detect the damage before it reaches the critical damage threshold so that the structure can be repaired and restored to its original strength.

The Current State-of-the-Art in Design and Analysis Methods

While significant improvements have occurred to structural design and analysis methodologies over the past two decades, the current standard practices used by the aerospace industry are still largely semi-empirical [for examples, see Refs. 12 and 13]. Finite element methods and sophisticated computer codes are used routinely to calculate very accurate stress, strain, and displacement fields for complex structures subjected to in-service, combined loads. Superior graphical interfaces have significantly improved pre- and post-processing of data files. Automated mesh generation, mesh refinement, and automated adaptive remeshing have resulted in major efficiencies in model development time, analysis time, and accuracy of the numerical solutions. Post-processing algorithms and graphical interfaces have significantly improved the ability of the analyst to interpret the results of the stress analysis. However, the prediction of structural failure modes, ultimate strength, residual strength of damage-tolerant structure, and fatigue life has remained elusive for the structural engineer. A rigorous structural analysis suitable for predicting structural failure requires the prediction of high-fidelity local stresses and local stress gradients that can be used with physics-based failure criteria and damage models. The global/local analysis method is one method currently under development to predict structural failure. A rigorous global/local analysis method must also include a progressive damage prediction capability to determine residual strength as damage propagates and fatigue life. The progressive damage analysis method must have the capability to predict the initiation and growth of damage due to the anticipated structural loading conditions and vehicle service environment. At the present time, rigorous analysis methods for metallic structures are much more mature than are the corresponding methods for composite structures [Ref. 12]. This observation is primarily attributed to the fact that fracture mechanics methods to predict the fatigue crack growth and fracture of metallic structures are in routine use throughout industry. In addition to the complexity of predicting damage initiation and growth in composite structure, nonlinear

structural response characteristics such as buckling, postbuckling, and pressurized structural deformations are also be predicted accurately. The analyses necessary to predict these nonlinear response characteristics must include the appropriate material properties for composite materials. Therefore, computational methods that rigorously account for material anisotropy must also be used to design composite structures.

Physics-based, rigorous progressive damage analysis (PDA) methods offer great potential to model failure modes accurately and to predict the residual strength of composite structures. However, these methods are not fully developed for all aerospace vehicle applications. A comprehensive state-of-the-art evaluation of progressive damage analysis methods was recently conducted by Soden, Hinton, and Kaddour [Refs. 14-16]. In Phase A, conducted between 1994 and 1997, 11 principal investigators participated in a comparative program led by a group of researchers at QinetiQ, formerly The Defence Evaluation and Research Agency, in the United Kingdom. The participants were provided a description of 15 test problems to be analyzed [Ref. 14]. These 15 test problems included several glass-epoxy and graphite-epoxy material systems, several fiber-dominated and matrix-dominated laminate stacking sequences, and several loading conditions including uniaxial and biaxial tension, compression, and shear. Each participant was given the same material property database for the constituents and required to provide predictions of the initiation of damage and laminate failure to the program organizers. The organizers then compared the predictions to the results obtained from an independently conducted experimental verification test program [Ref. 15]. In Phase B of the study conducted between 1998 and 2002 [Ref. 16], the principal investigators were provided the results of Phase A and given an opportunity to modify their failure models and make refined predictions. In both Phase A and Phase B, the model predictions varied widely, with some significant discrepancies from the experimental results. These differences were primarily attributed to the lamina level failure criteria employed by the various models, treatment of residual thermal stresses, and treatment of final failure modes and mechanisms. Several general conclusions may be stated from this study. Physics-based failure criteria are still primitive. Loading history dependent damage evolution laws do not exist or are empirical. Most models do not have a complete representation of all failure modes, complex damage states, and combined stress states. Finally, progressive damage analysis methods are currently a researcher's tool, and reliable, verified, user-friendly engineering tools are not yet readily available.

The status of several advanced design and analysis methods with the attributes described above are explored in the following sections. The capability of these advanced methods will be illustrated by presenting the results of two recently completed NASA technology development programs. These programs include the X-33 hypersonic test vehicle demonstrating technologies for a single-stage-to-orbit space launch vehicle, and the NASA Advanced Subsonic Technology (AST) Program demonstrating technologies for large transport aircraft. The X-33 Program was selected because it illustrates the ability of expert engineers to use current analysis methods to explain the unanticipated structural failure of a complex, all-composite, all-bonded honeycomb sandwich structure. The computational results presented in the next section were performed in support of the official NASA Failure Investigation Board. The second example is the AST Program. The results of the AST Program illustrate the damage tolerance of a composite wing structure with a saw cut simulating discrete source damage and undetectable impact damage at several locations. In addition, the AST Program results also illustrate the state-of-the-art in

predicting the residual strength of an aircraft fuselage subjected to a simulated discrete source damage.

Failure Analysis of the X-33 Liquid Hydrogen Cryotank

The objective of the X-33 experimental rocket-powered vehicle, see artist rendering in Figure 7, is to demonstrate critical technologies for a reusable launch vehicle at hypersonic flight approaching Mach 13. Among these technology demonstration goals is a liquid hydrogen (LH2) tank fabricated from composite materials. The vehicle configuration showing the location of the LH2 tanks and the tank construction details are shown in Figure 8. The LH2 tank is a complicated four-lobe (quadrant) conical shell with a noncircular cross-section and a non-spherical two-lobe end cap [Ref. 17]. The tank shell is a sandwich construction with composite inner and outer face sheets and a composite honeycomb core. The outer face sheet is a 7-ply, IM7/977-2 laminate (0.034-inch [0.864-mm] thick) with stacking sequence $[65/0/-65/90/-65/0/65]_T$. The core is a 1.5-inch- (38.1-mm-) thick Korex honeycomb material with a 3/16 cell width and with a 3.0 pounds per cubic foot density. The inner face sheet is a 13-ply, IM7/977-2 laminate (0.066-inch [1.68-mm] thick) with stacking sequence of $[45/90_3/-45/0_3/-45/90_3/45]_T$. The internal stiffening substructure is fabricated from textile preform graphite/epoxy composite materials. The all-composite, all-bonded tank was assembled using a complex, nine-step 350° F (177° C) curing and bonding procedure.

Unfortunately, the tank failed during the (protoflight) ground structural proof test [Ref. 17]. The structural failure occurred while the empty tank was warming to ambient conditions after completion of a series of successful pressurization and mechanical loads tests. (In addition to the internal pressure required to maintain the cryogen, the vehicle thrust loads during launch are transferred directly through the LH2 tank.) Referring to Figures 9 and 10, the lobe failure was characterized by a major debond between the honeycomb core and the inner skin of the sandwich. The lobe was partially debonded along the longeron between lobes number 1 and number 4 and the circumferential stiffening ring between the conical body of the tank and the hemispheric dome.

There were several primary causes that led to the structural failure of the tank. First, the as-manufactured bond strength between the honeycomb core and the inner face sheet of the tank lobes, Figure 11(a), was lower than expected. Second, foreign object debris (FOD) was inadvertently left on the bondline, Figure 11(b). The post-test visual examination of the core to inner face sheet bondline revealed the presence of two pieces of FOD. These FOD were found to be E. I. DuPont de Nemours, Inc., Teflon tape, which was used during the tank fabrication process. And third, the structural designers had an incomplete understanding of the permeability of liquid hydrogen through composite materials. The pressures in the honeycomb core of each of the four lobes measured during earlier tank pressurization tests revealed a rise in core pressure that correlated with the tank internal pressure. This response indicated that the tank pressure boundary had been breached. The failure investigation found an extensive network of microcracks in every ply of the inner skin, see Figure 11(c), that may have provided a leak path for the LH2. Finally, just prior to the catastrophic failure of lobe number 1, the core of each lobe of the tank exhibited a significant rise in pressure. This behavior is similar to the classic cryopumping phenomenon sometimes exhibited by open cell honeycomb sandwich cryogenic

pressure vessels. When the tank was pressurized, the crack network opened and allowed LH2 to leak into the core cells. When the pressure in the tank was released, the crack network closed and trapped the LH2 in the core cells. When the trapped LH2 heated sufficiently, the LH2 changed to hydrogen gas and increased the pressure in the core cells enough to fail the tank.

A fracture mechanics analysis of the region with the FOD was conducted to estimate the critical core pressure for unstable debond growth. Debond analyses were performed assuming that there were various shaped debonds existing between the core and inner face sheet. The three-dimensional finite element method [Ref. 18] was used to analyze the problem. The ABAQUS general-purpose finite element computer code was used to perform all computations. The materials were assumed to be linear elastic; and geometrically nonlinear analyses were performed. Two types of panel configurations, flat and curved, were considered. First, a square panel with 12-inch (304-mm) side lengths and a rectangular debond of size $a \times b$ as shown in Figure 12(a) was considered. Various size and aspect ratio debonds were analyzed. The sandwich panel was subjected to a pressure, P , within the core. Next, a curved panel with a radius of curvature of 48 inch (1.22 m) was analyzed, Figure 12(b). For both the flat and curved panel models, the sandwich was modeled using 20-node quadratic hexahedron finite elements, Figure 12(c). One element through the laminate thickness was used for the outer and inner face sheets. The core was modeled with four elements of unequal thickness. Near the debond front, the models were made such that the element sizes ahead and behind the debond fronts were identical to facilitate the calculation of the strain-energy release rates. The strain-energy release rates at stations along the debond front were calculated using the virtual crack closure technique (VCCT) [Ref. 18]. In the VCCT, the forces at and near the debond front are used in conjunction with the relative displacements behind the debond front to compute the strain-energy release rate.

The finite element (FEM) models were calibrated using experimental data obtained from single cantilever beam (SCB) test results. SCB test specimens were taken from a spare lobe identical to the failed tank, which had not been assembled on the second tank during fabrication. Values of fracture toughness (critical strain energy release rate) were measured using the standard compliance calibration test method, see insert in Figure 13. These test data are plotted in the bar chart shown in Figure 13. (Complete details of the test program may be found in Reference 17). Values of strain-energy release rates computed from the FEM models were particularly sensitive to the bending modulus of the face sheet laminates. Because of uncertainty in the material property data, the more critical material properties for the FEM model were chosen so that the results from the FEM model matched the measured values from the SCB results. The correlation between the FEM model and the SCB test results is shown in Figure 14. To calculate strain-energy release rates, the critical load was determined at each debond length used in the SCB tests. Correlating the FEM model results to the experimental values provided a consistent set of stiffness properties to be use in the FEM model for predicting the strain-energy release rate for the region where the FOD was found in the failed lobe.

Two special tests were conducted to verify the failure prediction accuracy of the FEM models. Two 12-inch (305-mm) by 2-inch (50.8-mm) sandwich panels were extracted from the spare lobe and a 1.0-inch (25.4-mm) by 2.62-inch (66.5-mm) rectangular debond was fabricated in the panels. The panels were tested to failure due to pressure applied into the core between the inner and outer face sheets. The debond between the core and inner face sheet was artificially

induced by cutting a section out of the inner skin. A patch equal to the thickness of the inner face sheet was used to repair the panel after forming the debond. Panel number 1 contained a core splice and Panel number 2 had a uniform core. SCB and flatwise tensile test specimens were also removed from the lobe location adjacent to the test panels. Local values of strength and fracture toughness were measured in the immediate vicinity of the test panels. The fracture toughness of Panel number 1 with the core splice was significantly higher than the value measured for Panel number 2. The dashed horizontal lines plotted in Figure 15 are the mean values of the fracture toughness (critical energy release rate or fracture toughness, G_{cr}) measured for the two test panels. An FEM model was built to represent the two test panels. The strain-energy release rates computed by the FEM analysis are plotted against core pressure in Figure 15. The predicted failure pressures are defined as the intersection of the G_{cr} line for each panel and the G versus pressure curve plotted in Figure 15. The actual failure pressures measured for the two test panels are plotted in Figure 15 using the star symbol. For Panel number 1 containing the core splice, the FEM model predicted a failure pressure of 158 psig (1.09 MPa) and the experimental failure pressure was measured to be 173 psig (1.19 MPa). For Panel number 2 with the uniform core, the FEM model predicted a failure pressure of 141 psig (0.972 MPa) and the experimental failure pressure was measured to be 128 psig (0.883 MPa). This excellent agreement between the FEM model predictions and the test results is within the numerical accuracy of the analysis method and within the scatter in the fracture toughness data.

The computational results for the region with the 1/2-inch- (12.7-mm-) wide, J-shaped Teflon tape FOD, shown in Figure 11(b), is presented in Figure 16. Three different debond sizes were analyzed because the exact dimensions of the debond cannot be determined from the photograph of the FOD. The most probable width of the debond produced by the Teflon tape is about 0.625 inches (15.9 mm). This estimate of the tape width is based on the observation that the tape cut through the weak thin cell wall regions where the honeycomb core is bonded to the inner face sheet. Since the exact local value of the core to inner face sheet fracture toughness at the Teflon tape FOD was not known, the mean value (mean- G_{cr}), three-sigma ($3\sigma-G_{cr}$) lower limit of the fracture toughness, and the lowest measured value of fracture toughness are plotted in Figure 16. Using the results plotted in Figure 16, the critical pressure for unstable debonding at the Teflon tape was between 100 psig (0.689 MPa) and 160 psig (1.103 MPa). There is also uncertainty about the exact pressure in the honeycomb core at the lobe failure location. Only a few core pressure values in each lobe were actually measured and the values ranged from 44 psig (0.303 MPa) to 66 psig (0.455 MPa). However, a chemical analysis of the gas trapped in the core of the three intact lobes revealed the presence of hydrogen. A detailed computational analysis of the pressures associated with the phase transformation of hydrogen from liquid to gas predicted core pressures from 108 psig (0.745 MPa) to 202 psig (1.393 MPa). Therefore, the failure investigation board could only conclude that the Teflon FOD might have been the initiation site of the failure.

Development of Technology for Composite Wings of Subsonic Transport Aircraft

The objective of the NASA AST Program was to develop and demonstrate advanced design and manufacturing technology for a cost-affordable composite wing of a large transport aircraft. The first major AST Program milestone was the design, fabrication, and testing of a wing stub box. The wing stub box was designed and fabricated by Boeing Company under

contract to NASA and tested by NASA Langley Research Center [Ref. 19]. The wing stub box was fabricated using graphite-epoxy textile materials (Hercules, Inc., AS4/3501-6 and IM7/3501-6) and stitched together using the E. I. DuPont de Nemours, Inc., Kevlar thread. The IM7 graphite fibers were used only for the 0-degree fibers in the lower cover panel skin. The composite skin and stiffeners were composed of layers of dry fiber textile preform that were pre-knitted in nine-ply-thick stacks with a quasi-isotropic stacking sequence. The resin film infusion (RFI) process was used to impregnate the dry fiber preforms with resin and the subsequent composite structures were cured in an autoclave. The wing stub box was a manufacturing trial part that was tested as part of the building-block design approach used for the wing program.

The wing stub box test program was conducted at NASA Langley Research Center. The composite test article, shown in Figure 17, was attached to a metallic extension box to provide a load transition section so that loads representative of a transport wing structure could be applied to the stub box. The test plan included several design limit load test conditions and a design ultimate load test of the stub box with impact damage. One of the primary test objectives was to demonstrate the damage tolerance attributes of the stitched textile preform technology for undetectable and barely visible foreign object impact damage. The comparison of the test results to finite element model predictions was excellent [Ref. 19]. For example, a comparison of the analytical prediction with the experimentally measured displacement of the tip of the test article is shown in Figure 18. The model accurately predicted the onset of buckling in the cover panels of the box. The box failed at only 93 percent of the design ultimate load, which was slightly less than expected. The post-test investigation determined that the failure was initiated by undetectable impact damage in the web and flange of a stringer that terminated near (but not at) the front spar. The cover panel was designed to account for compression-after-impact conditions, but the damaged stringer added a transverse shear load component to the locally damaged area of the cover panel. This local shear load component created a local combined load condition in the damaged area of the cover panel. This test highlighted the sensitivity of composite structures to undetectable impact damage in regions of load redistribution such as the stringer termination. As a result of this outcome, the wing cover panels were redesigned to account for the more complex loading condition at the stringer terminations, and the redesigned features were included in a subsequent semi-span wing design described in the following paragraphs.

June 1, 2000, marked the formal completion of the AST Program with the successful test of a 42-foot- (12.8-m-) long Stitched/Resin Film Infused (S/RFI) Composite Wing Box [Ref. 20]. The objectives of the program were to demonstrate cost-affordable manufacturing technology for large-scale composite structure and to assess the suitability of current structural design methods. The wing box was designed and fabricated by the Boeing Company under contract to NASA to satisfy the requirements of a 220-passenger commercial transport aircraft. In the S/RFI manufacturing process, layers of multi-axial warp-knit graphite/epoxy fabric were stitched together using Kevlar thread, and then impregnated and cured using the resin film infusion process. The wing box was fabricated from Hercules, Inc., IM7 and AS4 fibers and 3501-6 epoxy. The upper cover panel consisted of nine-ply quasi-isotropic laminates assembled together in pre-knitted stacks. The lower cover panel was composed of alternating unidirectional 0° layers of IM7 fibers and ±45° and 90° layers of AS4 fibers assembled in pre-knitted stacks. The stiffeners, spars, and ribs were fabricated from the same materials. The components of the

wing box were stitched together using the E. I. DuPont de Nemours, Inc., Kevlar thread and then cured using the S/RFI process.

The full-scale wing box test program was conducted at NASA Langley Research Center. The test set-up is shown in Figure 19 for the wing box subjected to a design limit load test condition. One of the primary test objectives was to demonstrate the suitability of damage tolerance design methods. In this test program, the test article was subjected to foreign object impact damage at several locations; and, also, saw cuts through the cover panels were made to simulate discrete source damage. The wing box was subjected to several design limit load (DLL) tests to measure structural response and to verify the accuracy of nonlinear finite element analysis procedures used to predict the wing box response. These tests included a 100 percent DLL test representative of a braked roll-out condition, a test with a 1-g down-bending condition, and a test with a 2.5-g up-bending condition. In addition, the wing was subjected to 7-inch- (17.8-cm-) long saw cuts, simulating discrete source damage, in the upper and lower cover panels. The wing box successfully supported the 70 percent DLL requirement with the saw cuts as required by the FAR Part 25 [Ref. 2]. Prior to the design ultimate load (DUL) test, the saw cuts were repaired by an airline maintenance contractor to restore the wing box to its original DUL capability. Also, prior to the DUL test, the upper and lower cover panels were subjected to local impact damage events with impact energies ranging from 83 to 100 ft-lbs (113 to 136 N-m) to simulate foreign object damage. Sections of the wing structure were nearly 1-inch- (2.54-cm-) thick and were subjected to average running loads greater than 24,000 lbs/in (4.20 MN/m). The wing box failed at 97 percent of the DUL requirement with unrepaired impact damage. Failure initiated at an unreinforced access port in the lower cover panel that was not near any impact damage site. This failure load was well within the prediction accuracy of the finite element model and data scatter of the material properties used in the analysis of this complex structure. The ability of the wing box to sustain discrete source damage and foreign object damage successfully demonstrated the robustness of the S/RFI composite manufacturing process and validates the damage-tolerance design methods in current use for primary composite aircraft structures.

Development of Technology for Composite Fuselages of Subsonic Transport Aircraft

The NASA AST Program also included the development of design and manufacturing technology for fuselage structures. Unlike the wing program, the fuselage program did not include full-scale technology demonstration tests. This lack of full-scale components was primarily because the technology readiness level for a composite fuselage structure is much lower than that for a wing structure. The goals of the fuselage program included the development of cost-affordable manufacturing technology, efficient structural design concepts, and design and analysis methods. The fuselage is particularly challenging from a structural design point of view because of the complex, combined loading conditions produced by the internal cabin pressure and the airframe body forces. In addition, the thin-shell nature of the fuselage coupled with the complex loading conditions results in highly nonlinear structural behavior. The design of the crown region of the fuselage is dominated by tension loads, the side (window belt) region by shear loads, and the keel region by longitudinal compression loads and circumferential tension loads. Because the fuselage crown is tension dominated, the design details are established by damage-tolerance design criteria, particularly the discrete source

damage requirement. As illustrated in Figure 20(a) and (b), the crown region was selected as the focus for developing advanced damage tolerance design methodology for the fuselage. This methodology was demonstrated by conducting tests of curved, stiffened panel. Descriptions of two failure analysis methods developed in the program are described in subsequent paragraphs. The first method is an adaptation of a semi-empirical method originally developed for metallic structure extended to composite structure. As a parallel effort, a more rigorous progressive damage method was developed that uses primitive materials level failure criteria rather than empirical fracture parameters determined at the structural level.

Experimental Verification of Standard Semi-Empirical Methods

The curved stiffened panel tested in this study has four stringers and three frames as shown schematically in Figure 20(b) [Ref. 21]. The panels have a 122-inch (3.10-m) radius, a 72-inch (1.83-m) length, and a 63-inch (1.60-m) arc width. The skin of the panel was fabricated from Hercules, Inc., AS4 graphite fiber and the matrix is Fiberite 938 epoxy using a tow placement procedure. The laminate stacking sequence contains two +45° plies, two -45° plies, two +60° plies, two -60° plies, three 90° plies, and two 0° plies. The stringers were fabricated from Hercules, Inc., IM6 graphite fiber and 3501-6 epoxy, using unidirectional prepreg tape. The stringer stacking sequence contains four 45° plies, four -45° plies, three 90° plies, and four 0° plies. The frames were fabricated from braided graphite fiber performs with Shell RSL 1895 resin and cured by the Resin Transfer Molding (RTM) process. The stringers were co-cured with the skin and the frames, were secondarily bonded to the skin. The frames had cutouts in the attachment flanges and webs to allow the stringers to pass through the frames.

The curved stiffened panel was tested with combined bi-axial tension loads in a special NASA Langley Research Center pressure box facility shown in Figure 20(c) [Ref. 21]. The test facility has the capability to apply axial tensile loads and internal pressure in controlled combinations that simulate the stresses and displacements in the fuselage crown of a transport aircraft. Axial loads are applied by hydraulic actuators connected to curved steel plates attached to the test panel. Internal pressure is applied to the panel by an air pressure source with a pneumatic control system. Circumferential loads that develop in the skin of the panel are reacted at each side of the panel by fixed beams. Hoop loads that develop in the panel frames are reacted by steel rods that are connected to each end of the frames. Reaction loads in the rods are measured by load cells. The rods are connected to turnbuckles that can be adjusted to insure that the proper loads are reacted through the panel frames.

A severe state of damage was induced in the panel to simulate a discrete source damage event to a fuselage. A 22-inch- (0.559-m-) long saw-cut notch was induced in both the skin and the central circumferential frame as illustrated schematically in Figure 20(b). The panel was loaded to failure by controlled internal pressure and axial tensile loads. The saw cut notch was carefully monitored to determine the load when the notch extended and to document the crack growth from the original saw cut notch. The test results are shown in Figure 21 where crack growth from the notch tip is plotted against the applied internal pressure acting on the panel. The lowest triangle at the beginning of the dashed line in Figure 21 corresponds to the applied pressure at the onset of observable stable damage progression (crack growth) in the test. The

upper triangle at the end of the dashed line represents the extent of crack extension at catastrophic failure of the panel. As is readily apparent, considerable stable crack extension (>10 inches) occurred before the panel failed.

The stable damage growth exhibited by the composite panel prior to catastrophic failure is similar to the behavior exhibited by panels fabricated from ductile aluminum alloys. This observation suggests that the classical R-curve fracture mechanics approach may be used to predict panel failure. A finite element analysis of the curved, stiffened panel was conducted using the R-curve method to predict crack extension and panel failure [Ref. 22]. The R-curve (resistance effect) method is a failure criterion that models stable crack growth as a function of crack length and the applied, far-field stress state [Ref. 23]. The resistance effect exhibited by ductile metallic structures and some composite structures is that the applied load must be increased to continue the crack growth after initiation. This stable crack growth may extend significantly before catastrophic failure occurs. (This behavior is in contrast to brittle fracture where catastrophic failure is characterized by unstable crack propagation after initiation.) R-curves are measured experimentally by determining the fracture toughness or critical strain energy release rate for panels with center notches. Since R-curve behavior exhibits a significant panel width effect, the experimental data must be measured for wide panels with crack lengths that represent the dimensions of the crack in the actual structure of interest. Therefore, the R-curve, plotted in Figure 22, was determined from flat panels with the same laminate stacking sequence as the curved, stiffened panel used in the verification test. The crack lengths ranged from 0.25 inches (6.35 mm) to 12.0 inches (305 mm) and the panel widths ranged from 12.0 inches (305 mm) to 60.0 inches (1.52 m). The results of this analysis are plotted in Figure 21 in comparison to the experimental results. As can be seen, the R-curve method yielded analytical results that were in close agreement to the test results. These results strongly suggest that the semi-empirical method can be used for structural design and analysis. The following section will present a more rigorous approach to predicting fracture of composite structures and will discuss in more detail the stable crack growth behavior exhibited by the panels of this test program.

Advanced Progressive Damage and Residual Strength Methods

A progressive damage and residual strength methodology has been developed by NASA [Ref. 24]. The methodology relies on a nonlinear, damage-dependent constitutive model that represents the effects of ply-level damage on the laminate stress-strain behavior [Refs. 25-27]. The constitutive model uses internal state variables (ISV) to represent the average effects of local deformation due to the various modes of microcrack damage. This concept is called continuum damage mechanics. The constitutive model predicts the formation of intraply matrix cracks and fiber fracture for monotonic tensile loading and tension-tension fatigue, the associated ply-level stress and strain states, and the residual strength of the laminate. In order to rigorously predict the initiation and growth of a delamination, three-dimensional stress states such as those at the laminate free edges must be calculated. The constitutive model currently does not have this capability. The model uses an empirical relationship and user specified information to account for the effects of delaminations on load redistribution in a laminate. The material property descriptions required for the constitutive model include only the standard ply stiffness and strength data determined in the conventional manner for classical lamination theory [Ref. 28].

Under monotonic tension loading, the model uses the fiber failure strain, ϵ_{11}^{cr} , and matrix failure strain, ϵ_{22}^{cr} , determined from unidirectional laminate data. The model also uses the matrix failure shear strain, γ_{12}^{cr} , determined from Iosipescu test [Ref. 29].

The damage-dependent constitutive equations are substituted into the laminate resultant force and moment equations. These equations are then substituted into the plate equilibrium equations resulting in a set of governing differential equations that can be integrated against variations in the displacement components. Following well-known finite element formulation procedures, the damage-dependent plate equilibrium equations [Ref. 24] are given by

$$[K] \{d\} = \{F_A\} + \{F_D\} \quad (1)$$

where $[K]$ is the original global stiffness matrix, $\{d\}$ is the global displacement vector, $\{F_A\}$ is the applied force vector, and $\{F_D\}$ is the damage induced force vector. Since the effects of damage are represented as damage-induced force vectors $\{F_D\}$ on the right hand side of equation (1), the element stiffness matrix need not be recalculated as damage progresses as long as the nonlinearity in the load-deflection curve is not large. The progression of damage is predicted by an iterative and incremental computational procedure that has been implemented into the NASA finite element testbed, Computational Mechanics Testbed (COMET) [Ref. 24]. (The progressive damage and residual strength methodology implemented into COMET will be hereinafter referred to simply as the “model.”) The equilibrium solution is obtained when the damage-induced force vector and the change in displacements become negligible. If the solution shows that equilibrium is established, then the load is incrementally increased. If equilibrium is not established, then iterations are performed with the load held constant. (This procedure is very similar to the classical approach for the incremental theory of plasticity.) During the iterative process, the strain in an element may exceed the failure strain; the state of damage is then extended; and the iterations continue until equilibrium is reached. Eventually a load level will be reached where equilibrium is not attainable. This value of load is then used to define the residual strength of the laminate.

An experimental program was conducted to verify the predictive capability of the progressive damage and residual strength model. The material system used for the test specimens was the Hercules AS4 graphite fiber and the Hexcel 938 matrix, and the laminate stacking sequence was $[-45/+45/0/90/-30/+30/0]_s$. This laminate is a candidate aircraft structural laminate designed for the crown region of the fuselage. Center notch tension (CNT) panels with a variety of panel widths and notch lengths were tested to failure with applied tension loads. Notch-tip damage in the CNT specimen was documented using x-ray radiography. A typical damage state was previously shown in Figure 4. The radiograph in this figure was taken at 89.6 percent of the catastrophic failure load of a 36-inch (91-cm-) wide CNT panel. A drawing of the CNT panel is displayed to the left of the radiograph, and the actual dimensions are given to aid in visualizing the extent of the notch-tip damage zone. A "dark black tear" extending from the notch tip was identified as fiber fracture. The surrounding shaded region was produced by a local delamination. The thin lines extending from the notch-tip correspond to matrix cracks in the off-axis plies. During the CNT test, the applied load and crack opening displacement (COD) at the center of the notch were recorded. At higher applied loads, a pronounced discontinuity in the load-COD record may accompany the formation of damage. The specimen was unloaded at

the occurrence of each of these discontinuities and an x-ray radiograph, such as the one shown in Figure 4, was taken. For each consecutive loading, additional damage did not occur until the load exceeded the value that resulted in the previous damage. The slope of the reloading curve was different after the damage formation, indicating the strain softening effect of the damage. This stable damage growth process is somewhat similar to the crack growth resistance effect exhibited by ductile aluminum alloys.

The progressive damage and residual strength model was used to predict the damage progression and the residual strength of the CNT panels [Ref. 30]. The extent of damage predicted by the model for the CNT panel shown in Figure 4 is presented in Figure 23. A schematic of the CNT panel is shown at the top left with a small box drawn around the notch-tip region that represents the approximate area covered by the mesh displayed to the right of the drawing. The shaded elements are used to illustrate the extent of damage predicted by the model at about 88 percent of the failure load. The damage contour in Figure 23(a) illustrates the ply-level fiber fracture in the elements near the notch-tip. Mode I and mode II matrix cracking are illustrated in Figures 23(b) and 23(c), respectively. These damage contours were drawn for an equilibrated solution and illustrate the capability of the model to represent stable damage growth. Fiber fracture has extended about 1.1 inch (2.7 cm) from the notch-tip. Mode I and mode II matrix cracks have progressed to about 1.3 inch (3.2 cm) and 1.2 inch (3.0 cm), respectively. Excluding delaminations, the predicted damage state illustrated in Figure 23 is qualitatively similar to the corresponding experimental damage state shown in Figure 4.

The analytical predictions of residual strength are plotted in Figure 24 and represented by the triangles [Ref. 30]. The experimental data, represented by the squares in Figure 24, are the average of the three replicate tests for the AS4/938 panels. Comparing the squares to the triangles, the analytical predictions are seen to be within about 10 percent of the experimental values. The fracture behavior exhibited by the CNT panels shows a significant panel width and notch size effect. This effect is best viewed by comparing the data to the classical linear elastic fracture mechanics (LEFM) prediction represented by the solid line in Figure 24. The value of fracture toughness used in the LEFM prediction was calculated from the residual strength of the specimen with a $2a/W$ ratio of $1/4$. The experimental values for the 9.0-inch- (22.9-cm-) notch are about 50 percent higher than the LEFM prediction. (This result is similar to the panel width effect exhibited by ductile aluminum alloys.) The model correctly predicts this increase in the residual strength of the wide panels.

These results show the capability of the progressive damage and residual strength model to accurately predict the fracture of notched laminates using only material properties determined from the standard unidirectional laminate and Iosipescu shear test methods. However, these methods are not fully developed for all aerospace vehicle applications. Most analytical models, including the above described model, do not have a complete representation of all failure modes, complex damage states, and combined stress states. Finally, these methods are still under development, and reliable, verified, user-friendly engineering tools are not available.

Concluding Remarks

All aerospace vehicles must be designed to be durable and damage tolerant. This requirement is particularly challenging to composite structural designers because composite structures fail differently than metallic structure. Therefore, the 65 years of successful experiences with the design of metallic structures cannot be directly transferred to the design of composite structures. Several important factors explain why composite structures fail differently than metallic structures. First, composite materials are not isotropic and homogeneous like most aluminum alloys. Second, composite materials are generally brittle and lack the inherent benefit of the ductility exhibited by aluminum alloys. Third, the initiation and growth of material-level damage and the failure modes of composite structure are not well understood and cannot be predicted accurately. Due to these complications, the current design and analysis methods are semi-empirical and rely heavily on the building-block approach for design and certification. In addition, the best design practices for composite structure are not fully understood by many engineers.

Accurate, reliable, and user-friendly computational methods, design optimization methods, and robust structural design concepts are under development to address the deficiencies of the current standard practices. In addition, more durable and damage tolerant material systems and manufacturing technologies are also under development for advanced aerospace vehicle applications. Several recently completed NASA technology development programs demonstrate the state-of-the-art in current design practices and illustrate the technology readiness levels of advanced methods under development. While much progress has been achieved, the design and analysis methodology for composite structures is not fully mature for all aerospace structural applications. Several general conclusions may be stated. First, semi-empirical methods coupled with advanced finite element analysis tools can be used to design damage tolerant composite structure. Second, physics-based computational methods are under development that will eventually enable a rigorous damage-tolerance design and analysis methodology (damage initiation, growth, and residual strength). Finally, satisfying advanced durability and damage-tolerance design and analysis requirements is very challenging and requires failure mechanics experts to guide the analytical work.

References

1. Dost, E. F, W. B. Avery, S. R. Finn, L. B. Ilcewicz, D. B. Scholz, and R. E. Wishart, "Impact Damage Resistance of Composite Fuselage Structures," Part 3 NASA CP 3229, Part 1, National Aeronautics and Space Administration, Hampton, VA 23681, 1993, pp. 205-229.
2. Anon., *Aeronautics and Space, Code of Federal Regulations, Title 14*, published by the Office of the Federal Register, National Archives and Records Administration, U. S. Government Printing Office, Mail Stop SSOP, Washington, DC 20402, 1996.
3. Polymer Matrix Composites, Mil-Handbook-17, Volume 3, Chapter 7, Damage Resistance, Durability, and Damage Tolerance, Department of Defense, U. S. A., December 12, 2001. (Copies may be obtained from the Standardization Document Order Desk, Bldg. 4D, 700 Robbins Avenue, Philadelphia, PA 19111-5094.)

4. Anon., General Fracture Control Requirements for Manned Spacecraft Systems, NASA-STD-5007, National Aeronautics and Space Administration, George C. Marshall Space Flight Center, Huntsville, AL 35812, March 13, 2001.
5. Rhodes, M. D., J. G. Williams, and J. H. Starnes, Jr., "Effect of Low-Velocity Impact Damage on the Compression Strength of Graphite-Epoxy Hat-Stiffened Panels," NASA TN D-8411, National Aeronautics and Space Administration, Hampton, VA 23681, April 1977.
6. Rhodes, M. D., J. G. Williams, and J. H. Starnes, Jr., "Effect of Impact Damage on the Compression Strength of Filamentary-Composite Hat-Stiffened Panels," *The Science of Advanced Materials and Process Engineering Series*, Vol. 23, "Selected Applications of Materials for Products and Engineering," pp. 300-319, SAMPE, 1978.
7. Starnes, J. H., Jr., M. D. Rhodes, and J. G. Williams, "Effect of Impact Damage and Holes on the Compressive Strength of a Graphite-Epoxy Laminate," *Nondestructive Evaluation and Flaw Criticality for Composite Materials*, ASTM STP 696, R. B. Pipes, Ed., American Society for Testing and Materials, 1979, pp. 145-171.
8. Williams, J. G., M. S. Anderson, M. D. Rhodes, J. H. Starnes, Jr., and W. J. Stroud, "Recent Developments in the Design, Testing and Impact-Damage Tolerance of Stiffened Composite Panels," *Fibrous Composites in Structural Design*, E. M. Lenoe, D. W. Oplinger, and J. J. Burke, Eds., Plenum Press, New York, 1980, pp. 259-291.
9. Rhodes, M. D., J. G. Williams, and J. H. Starnes, Jr., "Low-Velocity Impact Damage in Fiber-Reinforced Laminated Epoxy Structures," *Polymer Composites*, Vol. 2, No. 1, January 1981, pp. 36-44.
10. Starnes, J. H., Jr. and J. G. Williams, "Failure Characteristics of Graphite-Epoxy Structural Components Loaded in Compression," *Mechanics of Composite Materials: Recent Advances*, Z. Hashin and C. T. Herakovich, Eds., Plenum Press, New York, 1983, pp. 283-306.
11. Jackson, W. C. and C. C. Poe, Jr., "The Use of Impact Force as a Scale Parameter for the Impact Response of Composite Laminates," *Journal of Composites Technology & Research*, Vol. 15, No. 4, Winter 1993, pp. 282-289.
12. Harris, C. E., J. C. Newman, Jr., R. S. Piascik, and J. H. Starnes, Jr., "Analytical Methodology for Predicting the Onset of Widespread Fatigue Damage in Fuselage Structure," *AIAA Journal of Aircraft*, Vol. 35, No. 2, March-April 1998, pp 307-317.
13. Harris, C. E., J. H. Starnes, Jr., and M. J. Shuart, "An Assessment of the State-of-the-Art in the Design and Manufacturing of Large Composite Structures for Aerospace Vehicles," NASA/TM-2001-210844, National Aeronautics and Space Administration, Hampton, VA 23681, April 2001.

14. Soden, P. D., M. J. Hinton, and A. S. Kaddour, "Lamina Properties, Lay-up Configurations and Loading Conditions for a Range of Fibre-Reinforced Composite Laminates," *Composites Science and Technology*, Elsevier, Vol. 58, 1998, pp. 1011-1022.
15. Soden, P. D., M. J. Hinton, and A. S. Kaddour, "A Comparison of the Predictive Capabilities of Current Failure Theories for Composite Laminates," *Composites Science and Technology*, Elsevier, Vol. 58, 1998, pp. 1225-1254.
16. Hinton, M. J., A. S. Kaddour, and P. D. Soden, "A comparison of the predictive capabilities of current failure theories for composite laminates, judged against experimental evidence," *Composites Science and Technology*, Elsevier, Vol. 62, 2002, pp. 1725-1797.
17. Anon., "Final Report of the X-33 Liquid Hydrogen Tank Test Investigation Team," National Aeronautics and Space Administration, George C. Marshall Space Flight Center, Huntsville, AL 35812, May 2000.
18. Raju, I. S., K. N. Shivakumar, and J. H. Crews, Jr., "Three- Dimensional Elastic Analysis of a Composite Double Cantilever Beam Specimen," *AIAA Journal*, Vol. 26, No. 12, 1988, pp. 1493-1498.
19. Wang, J. T., D. C. Jegley, H. G. Bush, and S. C. Hinrichs, "Correlation of Structural Analysis and Test Results for the McDonnell Douglas Stitched/RFI All-Composite Wing Stub Box," NASA TM 110267, National Aeronautics and Space Administration, Hampton, VA 23681, July 1996.
20. Jegley, D. C., and H. G. Bush, "Structural Testing of a Stitched / Resin Film Infused Graphite-Epoxy Wing Box," NASA TM 210846, National Aeronautics and Space Administration, Langley Research Center, Hampton, VA 23681, April 2001.
21. Rouse, M., D. R. Ambur, and J. T. Wang, "Evaluation of Damaged and Undamaged Fuselage Panel Responses Subjected to Internal Pressure and Axial Load," 6th NASA/DoD Advanced Composite Technology Conference, NASA CP 3326, Volume I, National Aeronautics and Space Administration, Hampton, VA 23681, 1996, pp. 685-700.
22. Wang, J. T., C. C. Poe, Jr., D. R. Ambur, and D. W. Sleight, "Residual Strength Prediction of Composite Fuselage Panel with Discrete Source Damage," 6th NASA/DoD Advanced Composite Technology Conference, NASA CP 3326, Volume I, National Aeronautics and Space Administration, Hampton, VA 23681, 1996, pp. 701-722.
23. Poe, Jr., C. C., C. E. Harris, T. W. Coats, and T. H. Walker, "Tension Strength with Discrete Source Damage," Fifth NASA/DoD Advanced Composites Technology Conference, NASA CP 3294, Volume I, National Aeronautics and Space Administration, Hampton, VA 23681, 1994, pp. 369-437.

24. Lo, D. C., T. W. Coats, C. E. Harris, and D. H. Allen, "Progressive Damage Analysis of Laminated Composite (PDALC) (A Computational Model Implemented in the NASA COMET Finite Element Code)," NASA TM 4724, National Aeronautics and Space Administration, Hampton, VA 23681, August 1996.
25. Allen, D. H., S. E. Groves, and C. E. Harris, "A Cumulative Damage Model for Continuous Fiber Composite Laminates with Matrix Cracking and Interply Delamination," Composite Materials: Testing and Design (8th Conference), ASTM STP 972, J. D. Whitcomb, Ed., American Society for Testing and Materials, Philadelphia, 1988, pp. 57-80.
26. Harris, C. E. and D. H. Allen, "A Continuum Damage Model of Fatigue-Induced Damage in Laminated Composites," *SAMPE Journal*, July/August 1988, pp. 43-51.
27. Lee, J. W., D. H. Allen, and C. E. Harris, "Internal State Variable Approach for Predicting Stiffness Reductions in Fibrous Laminated Composites with Matrix Cracks," *J. of Composite Materials*, Vol. 23, December 1989, pp. 1273-1291.
28. Jones, R. M., *Mechanics of Composite Materials*, Hemisphere Publishing Corporation, 1975.
29. Coquill, S. L. and D. F. Adams, "Mechanical Properties of Several Neat Polymer Matrix Materials and Unidirectional Carbon Fiber-Reinforced Composites," NASA CR 181805, National Aeronautics and Space Administration, Hampton, VA 23681, April 1989.
30. Coats, T. W. and C. E. Harris, "A Progressive Damage Methodology for Residual Strength Predictions of Notched Composite Panels," *J. of Composite Materials*, Vol. 33, No. 23, 1999, pp. 2193-2224.



(a) Widespread Fatigue Damage, Aloha Airlines Boeing 737, April 28, 1988



(b) Uncontained Engine Failure, Delta Airlines MD-88, July 6, 1996

Figure 1. Commercial transport aircraft are designed to be damage tolerant.

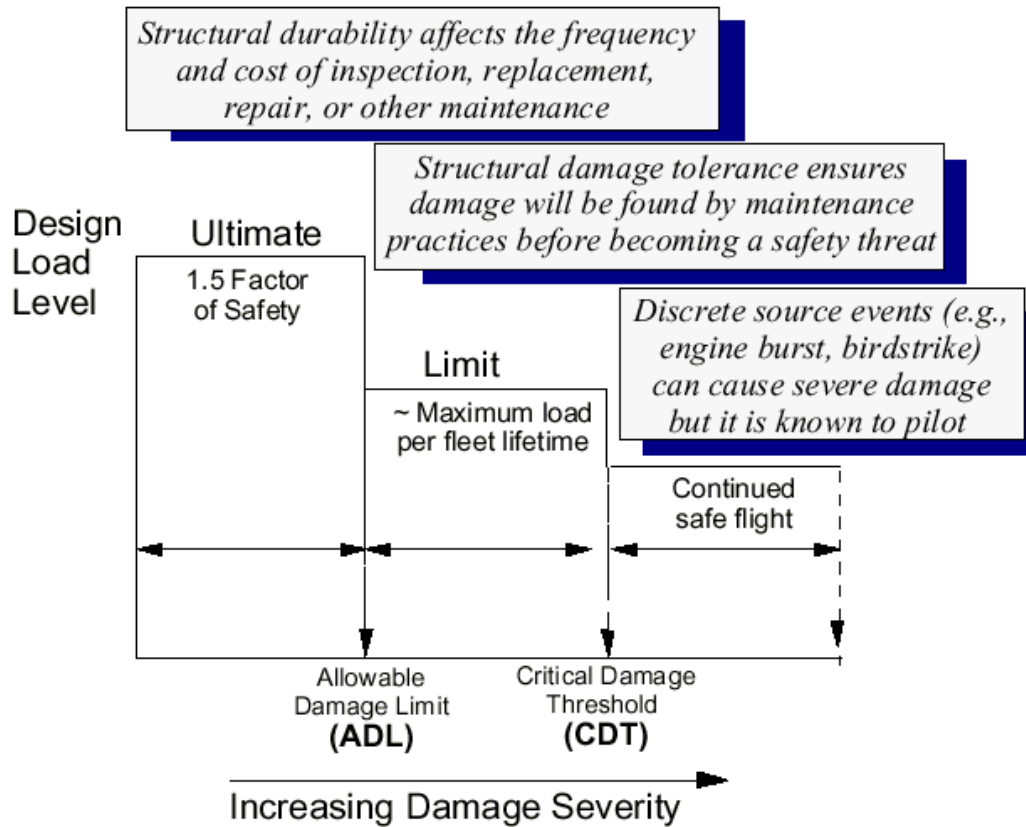
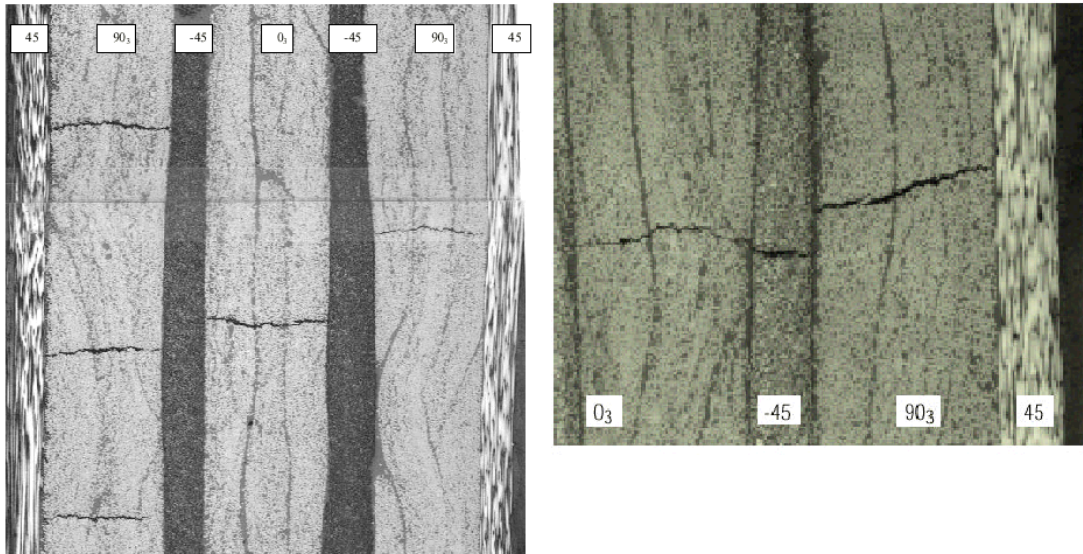


Figure 2. Definitions of durability and damage tolerance for commercial aircraft and associated design requirements (Mil-Hk-17).

Sections taken at 45 degrees to the 0 degree fiber direction



Graphite/epoxy, IM7/977-2, $[45/90_3/-45/0_1/-45/90_3/45]_T$

Figure 3. Examples of microstructure damage at the ply level of a laminate.

AS4 / 938 $(\mp 45 / 0 / 90 / \mp 30 / \bar{0})_S$

Far-field strain = 0.00205
(89.6% of failure)

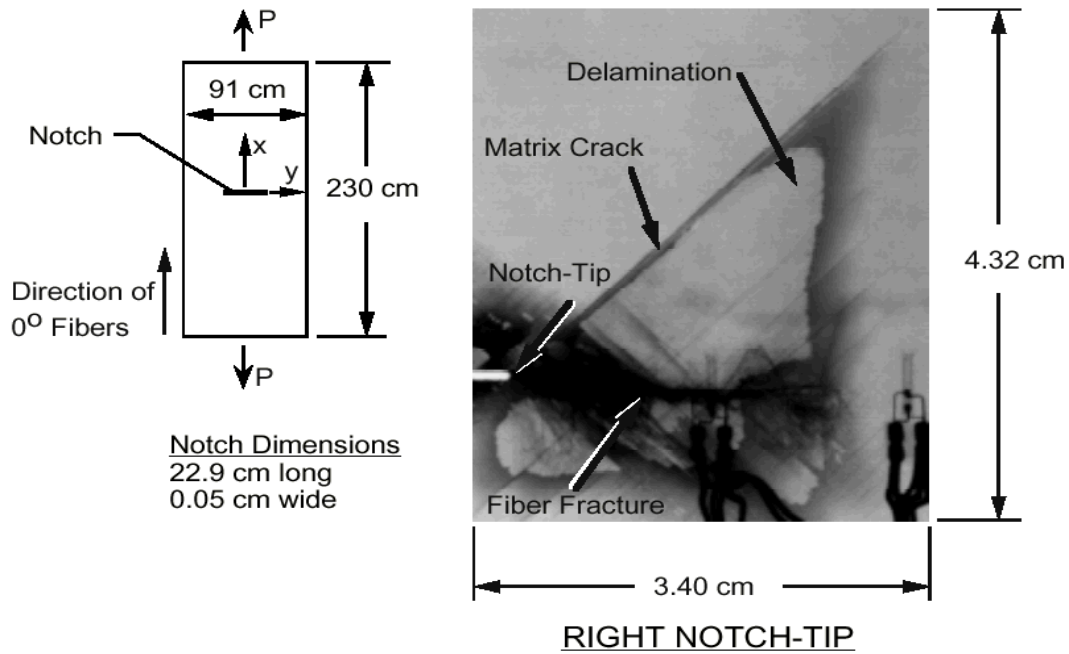
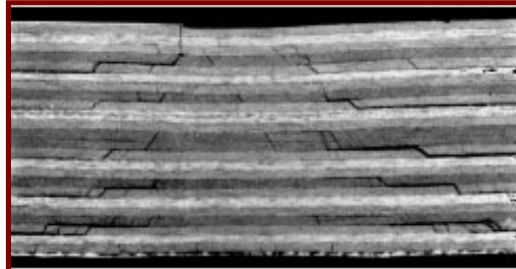


Figure 4. An example of the complex damage state in a laminate that may form at a hole or notch.

(a) Micrograph
(edge view of laminate)



(b) Ultrasonic Scan
(top view of laminate)

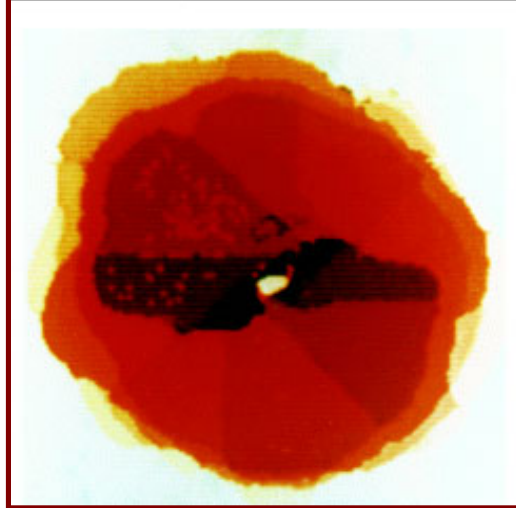


Figure 5. Foreign object impacts may produce complex, hidden damage states.

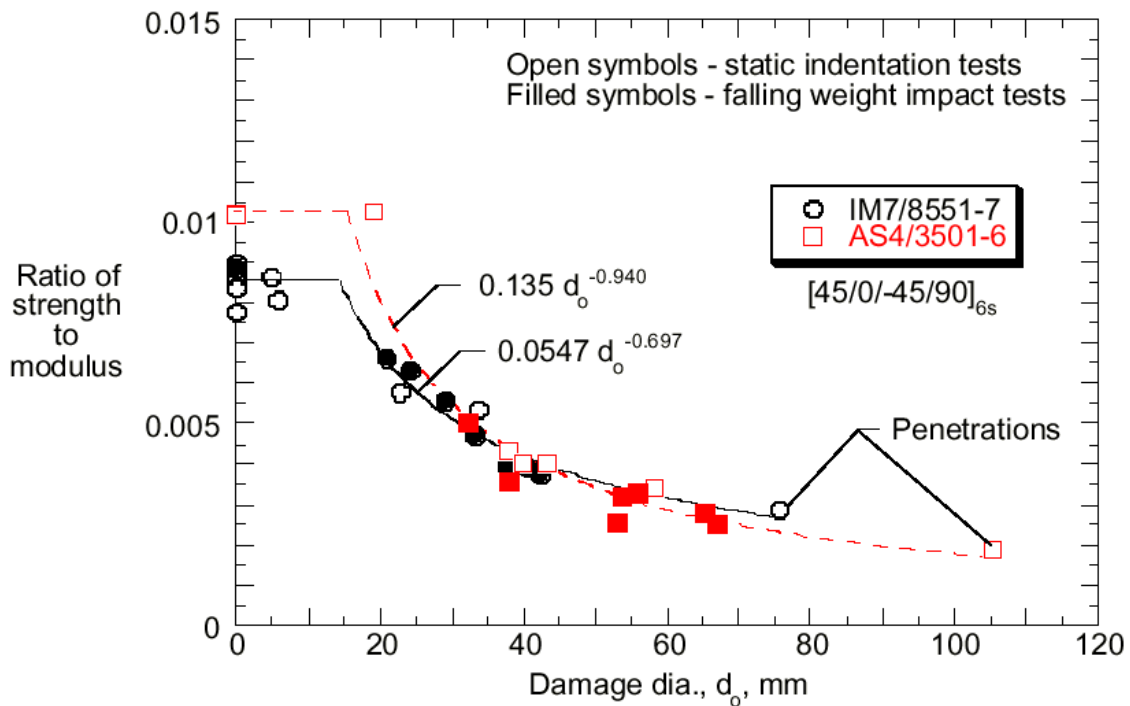


Figure 6. Compression-after-impact test data shows reduction in residual strength due to foreign object impact damage.



Figure 7. Artist rendering of the NASA X-33 hypersonic experimental vehicle.

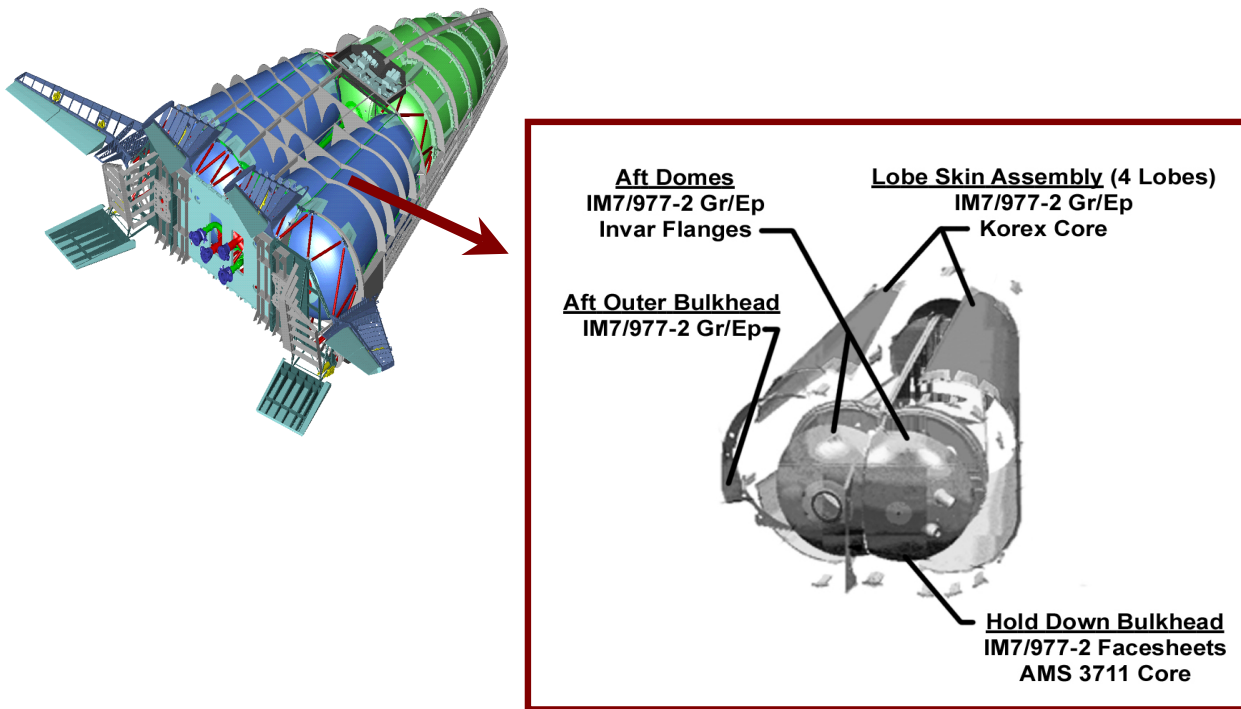


Figure 8. X-33 vehicle schematic shows the two side-by-side LH2 tanks and the LH2 tank construction details.

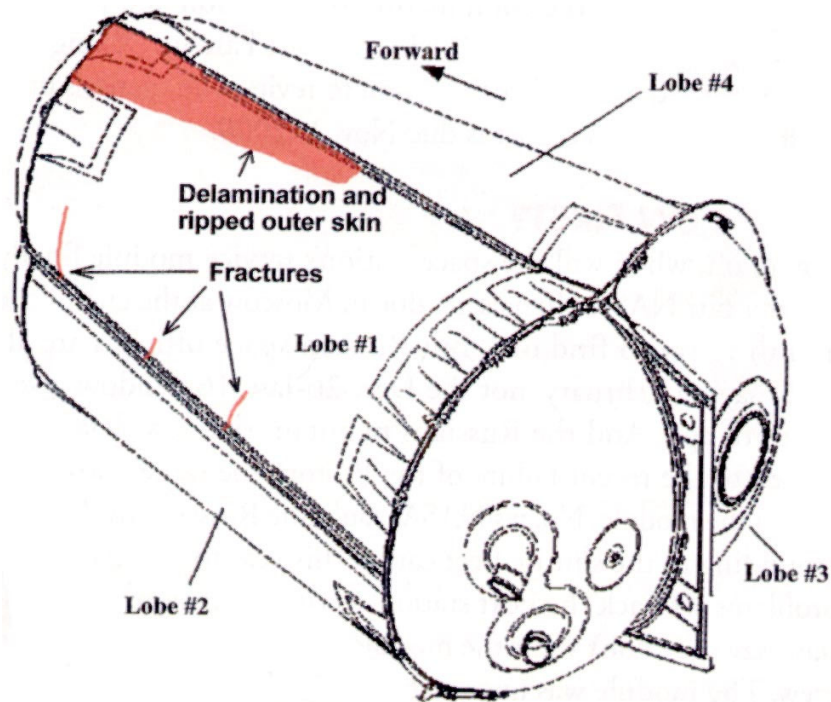


Figure 9. Schematic shows the location of the failed lobe of the X-33 LH2 tank.

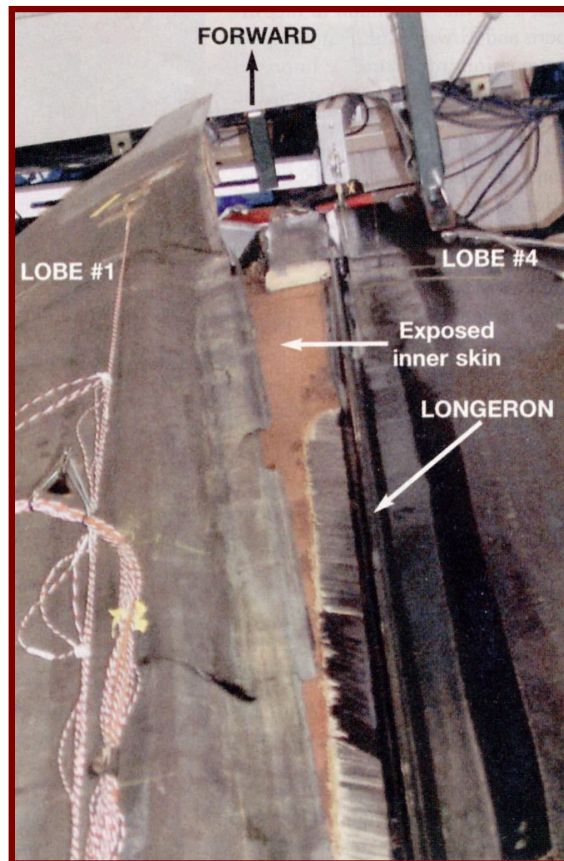


Figure 10. Photograph shows actual failure of X-33 LH2 honeycomb structure.

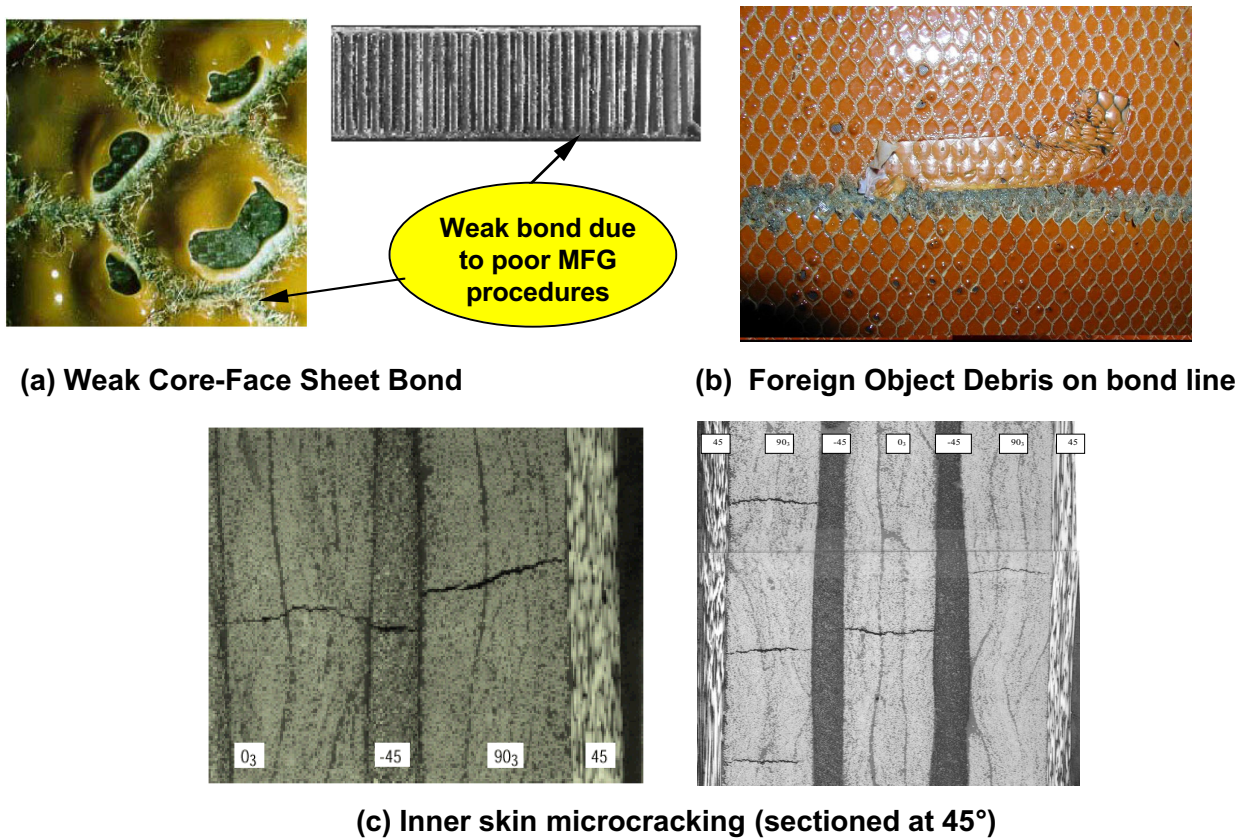


Figure 11. Three causes that led to the X-33 LH2 composite tank failure.

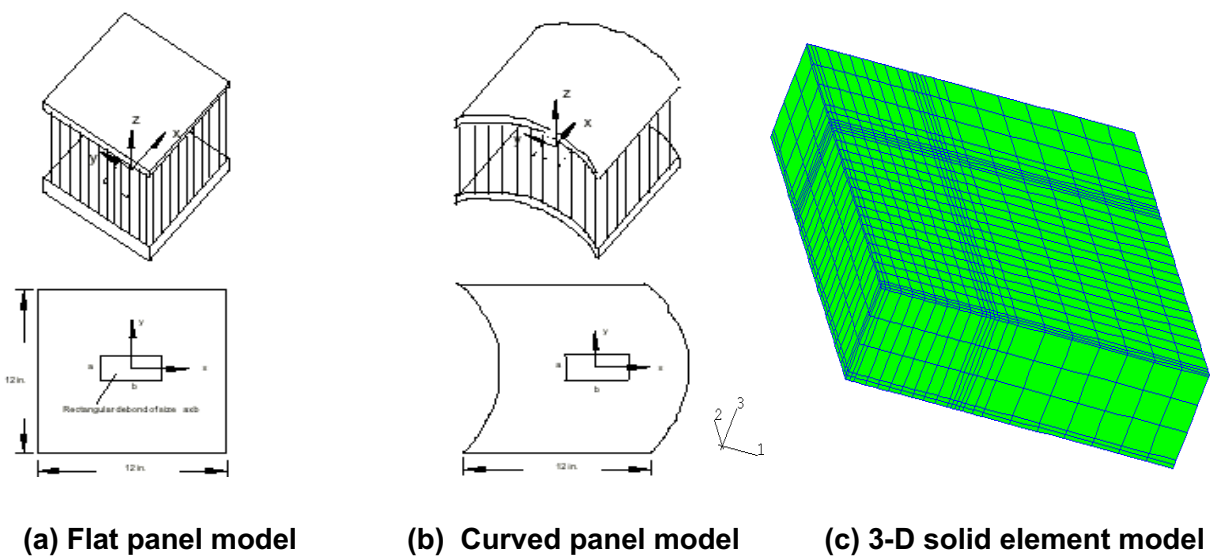


Figure 12. Schematics of the three-dimensional finite element models used to conduct the post-failure analysis of the X-33 LH2 tank.

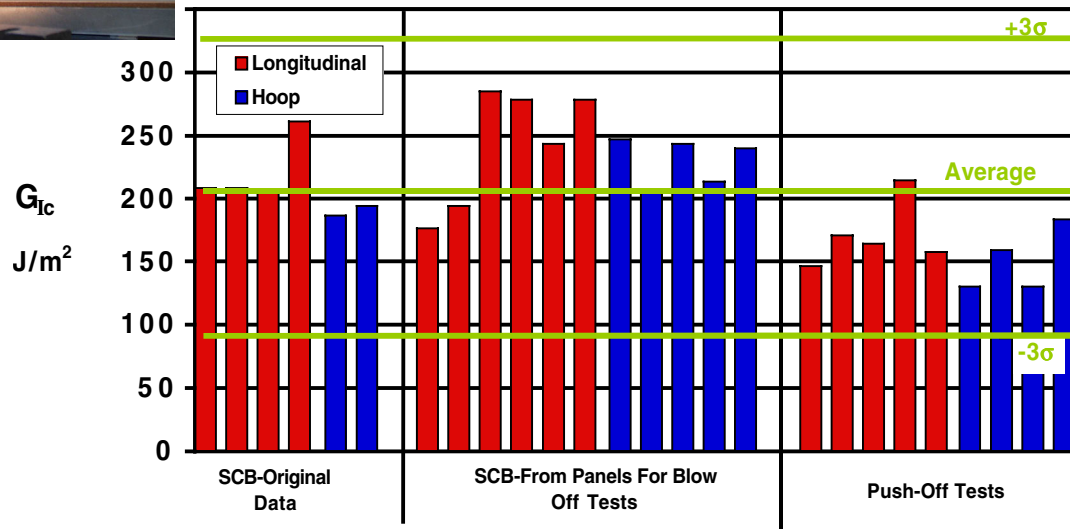
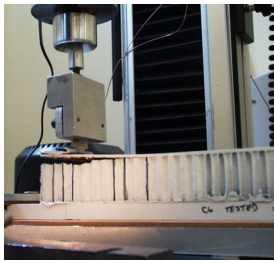


Figure 13. The honeycomb core disbond fracture toughness was measured using a cantilever beam specimen and the compliance calibration test method.

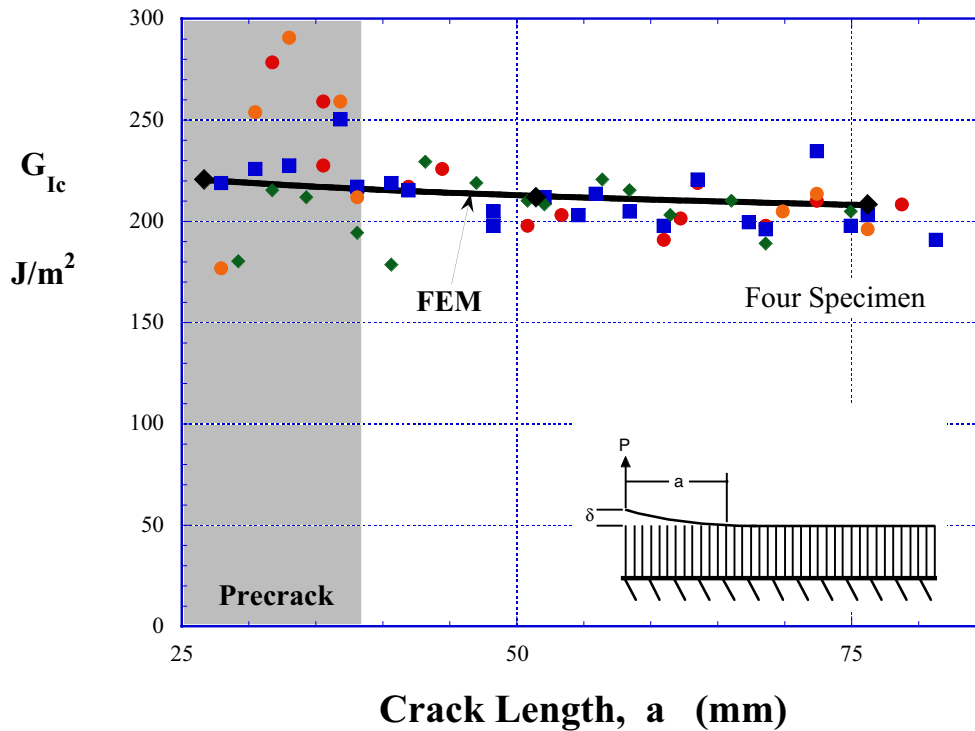


Figure 14. Correlation between the experimentally determined values of fracture toughness and the finite element model predictions.

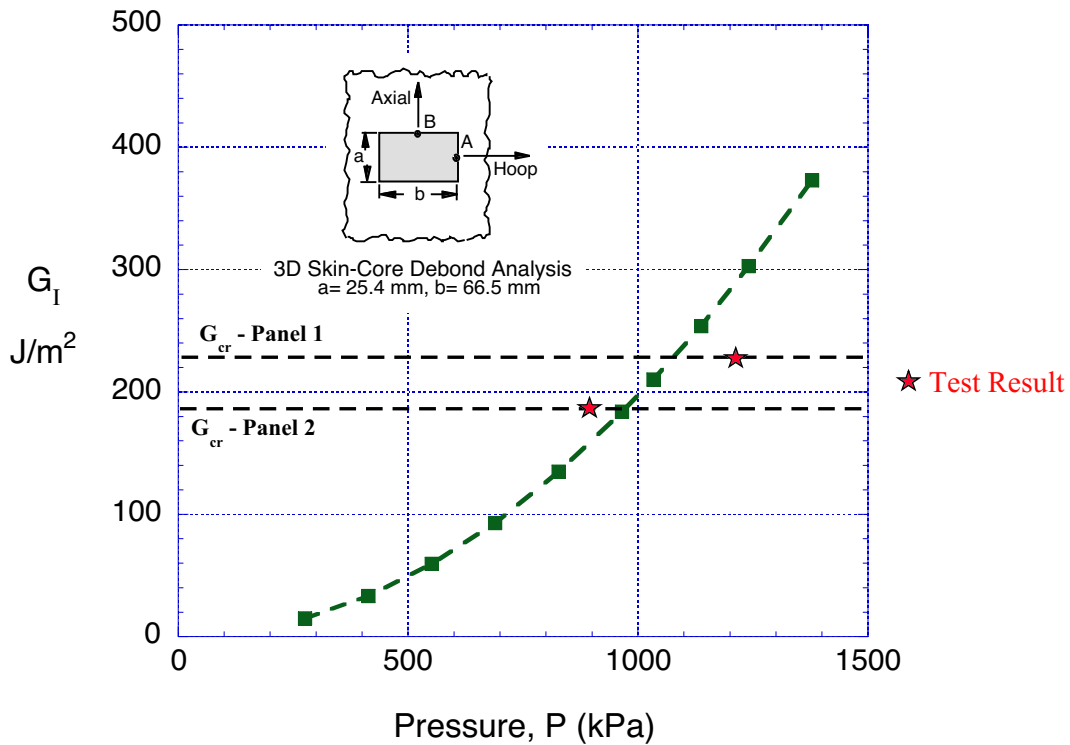


Figure 15. Comparison of the predicted critical pressure to the experimental results from the panel blow-off tests conducted to verify the analysis method.

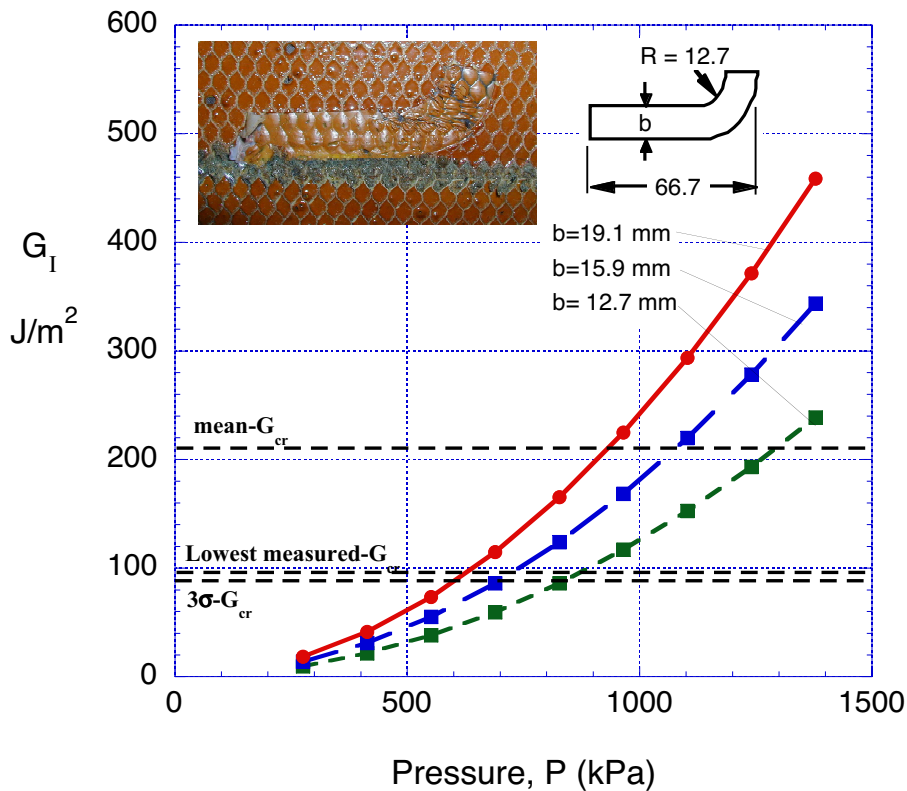


Figure 16. Strain energy release rate versus pressure in the honeycomb core for the foreign object debris discovered on the core-to-facesheet bondline.

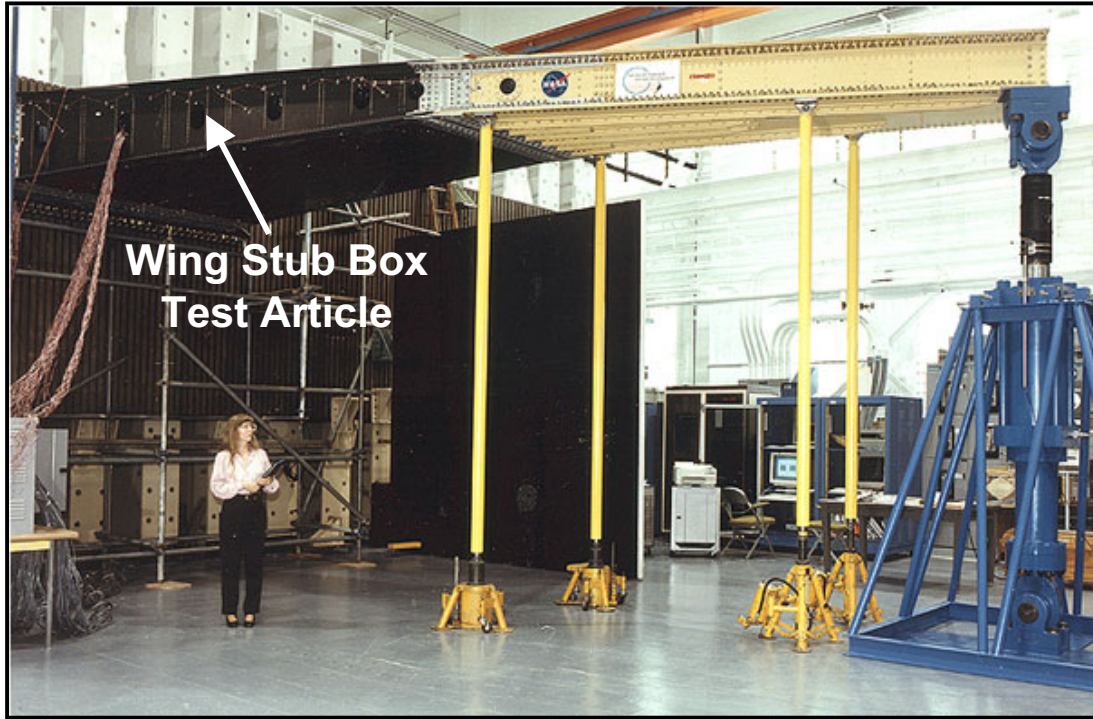


Figure 17. Wing stub box in NASA Langley Research Center test fixture.

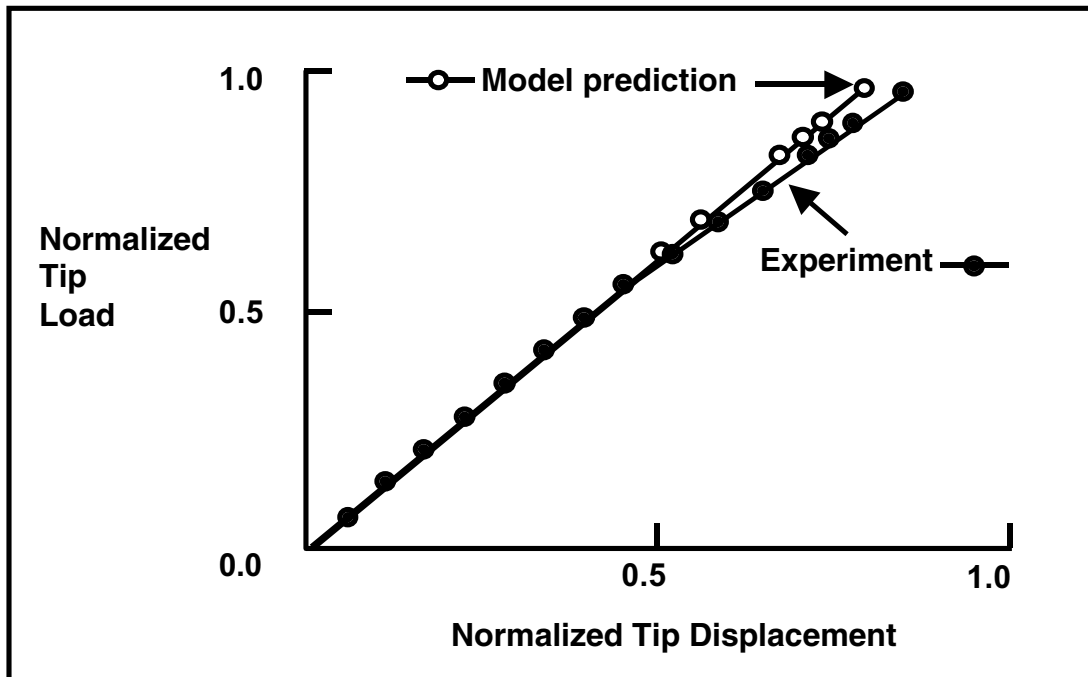
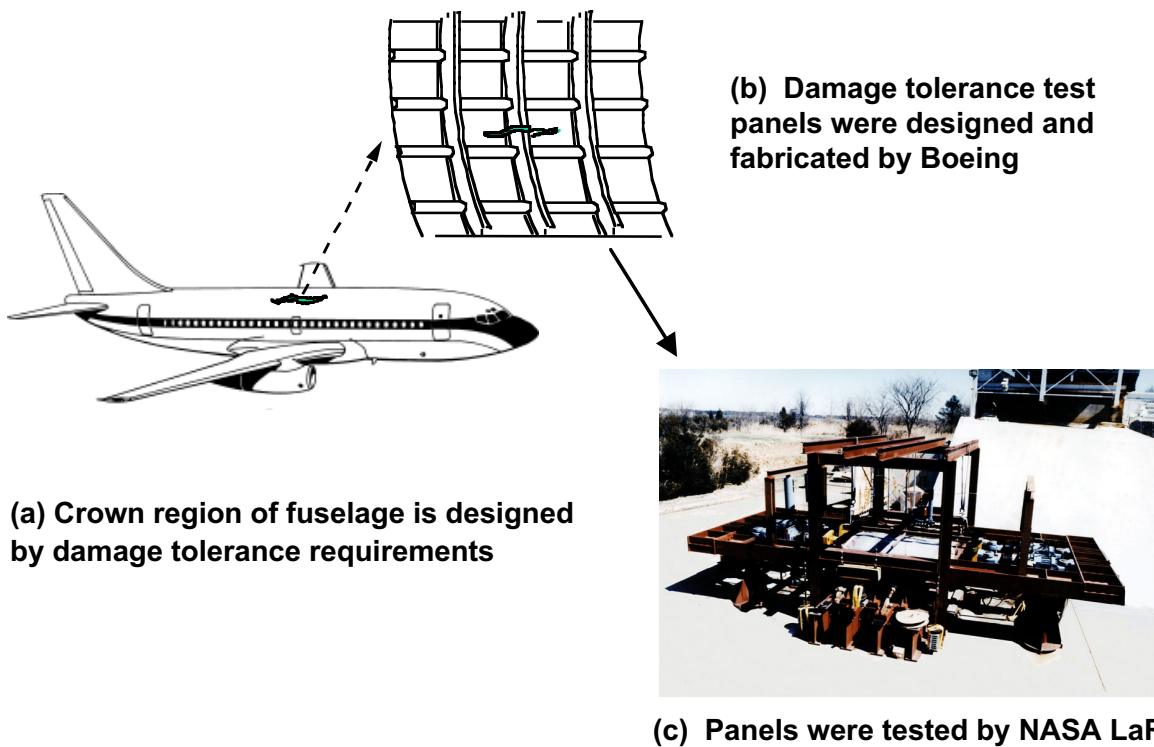


Figure 18. Comparison of Wing stub box test result to model prediction.



Figure 19. A full scale test of a composite wingbox was conducted by NASA to verify manufacturing scale-up methods and advanced design methods.



(a) Crown region of fuselage is designed by damage tolerance requirements

(c) Panels were tested by NASA LaRC

Figure 20. Component tests were conducted by NASA Langley Research Center to verify advanced damage tolerance methods for fuselage structure.

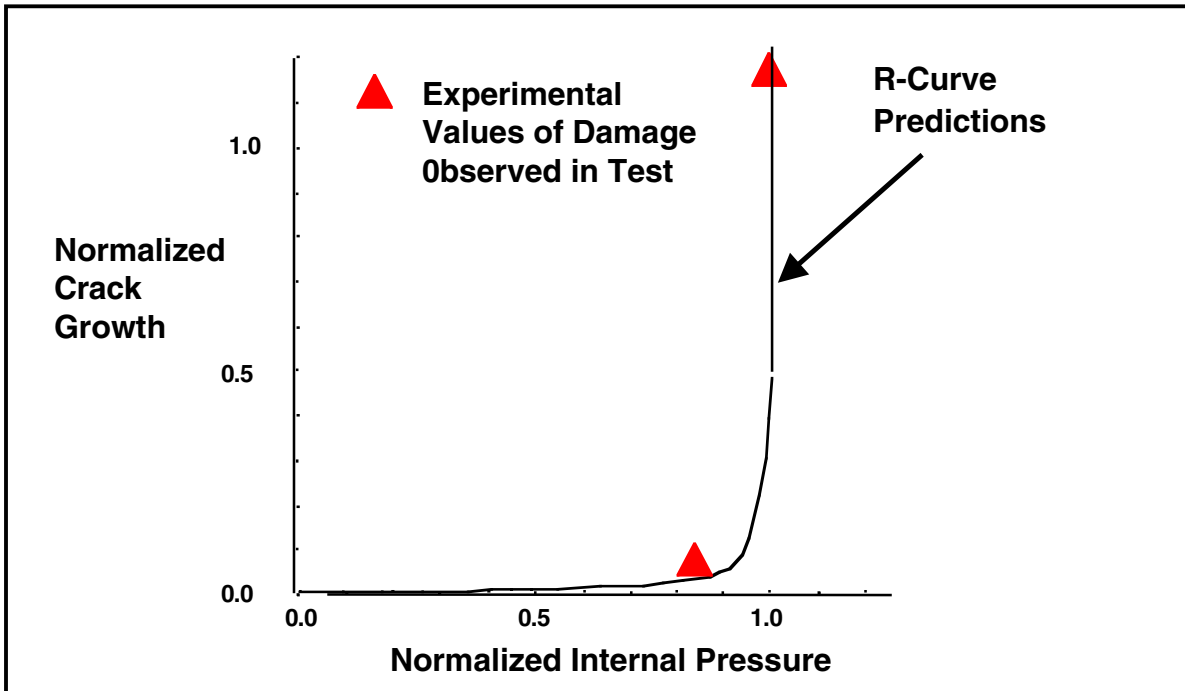


Figure 21. Comparison of the analytical method (R-curve) predictions to the NASA Langley Research Center component test results.

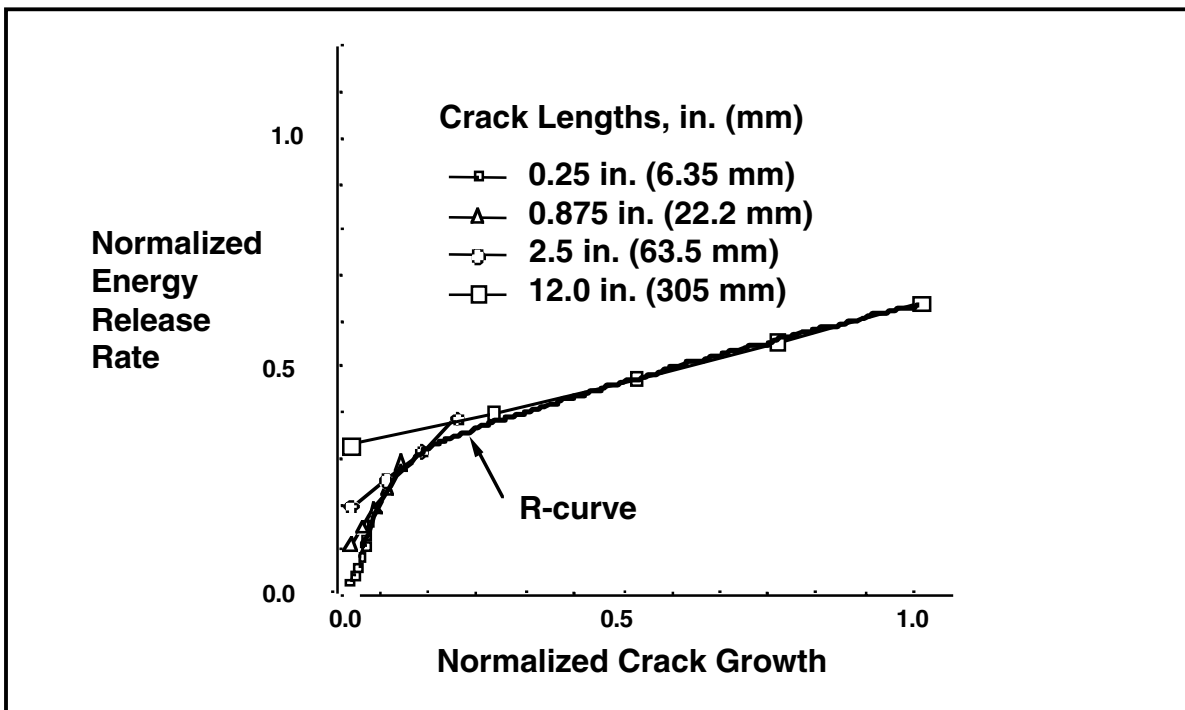


Figure 22. R-curve determined experimentally from laminate test data.

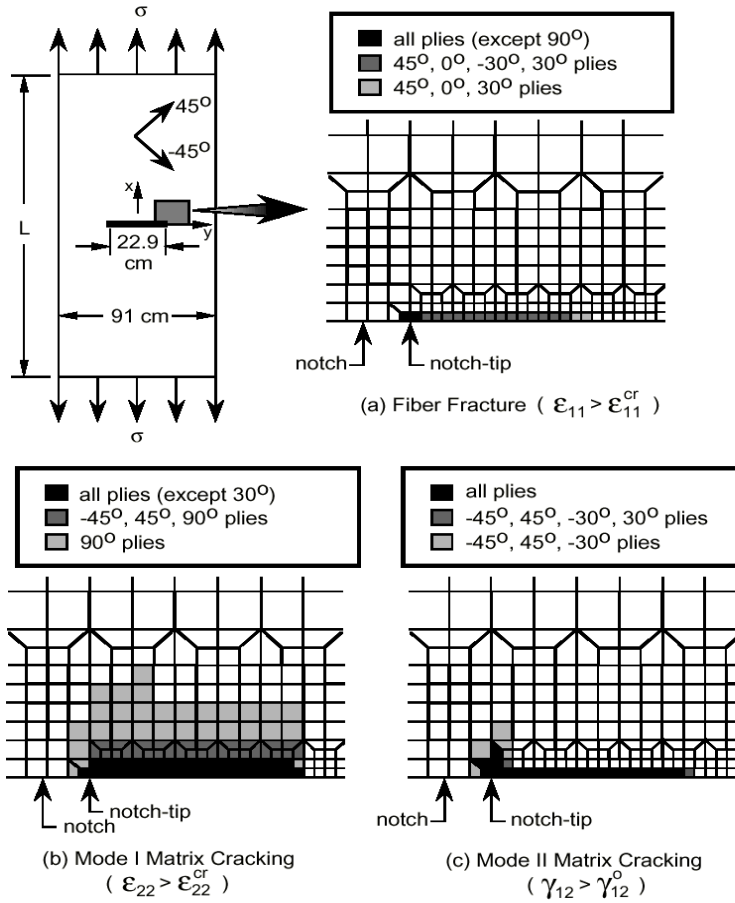


Figure 23. Model predictions of damage progression.

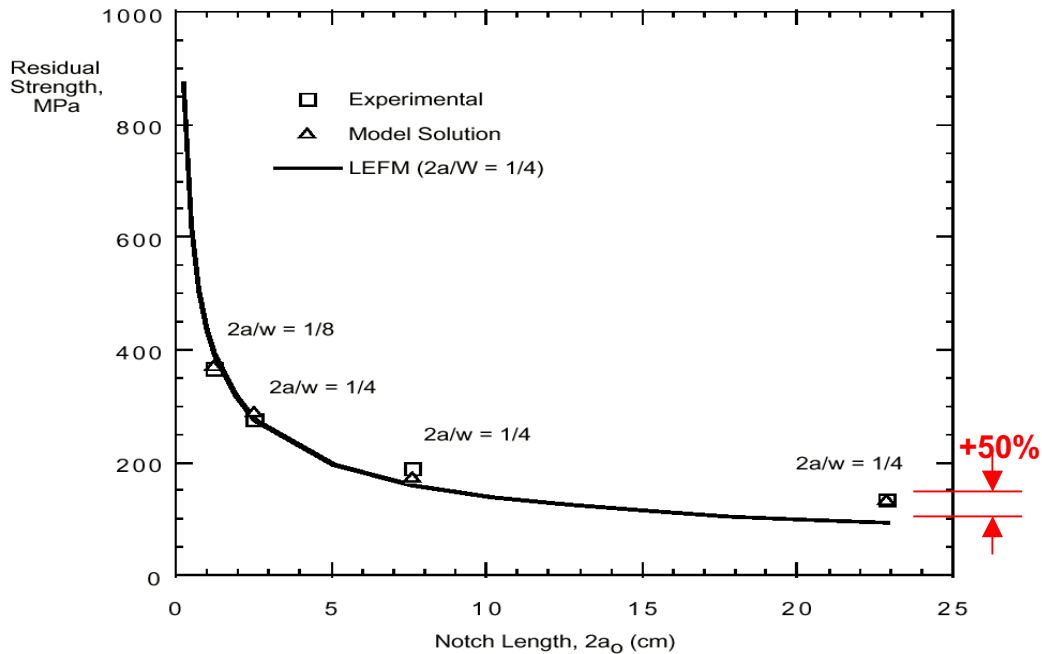


Figure 24. Comparison of predictions of residual strength to results from a wide panel tensile test program conducted by NASA.

| REPORT DOCUMENTATION PAGE | | | Form Approved OMB No. 0704-0188 |
|--|--|---|------------------------------------|
| Public reporting burden for this collection of information is estimated to average 1 hour per response, including the time for reviewing instructions, searching existing data sources, gathering and maintaining the data needed, and completing and reviewing the collection of information. Send comments regarding this burden estimate or any other aspect of this collection of information, including suggestions for reducing this burden, to Washington Headquarters Services, Directorate for Information Operations and Reports, 1215 Jefferson Davis Highway, Suite 1204, Arlington, VA 22202-4302, and to the Office of Management and Budget, Paperwork Reduction Project (0704-0188), Washington, DC 20503. | | | |
| 1. AGENCY USE ONLY (Leave blank) | 2. REPORT DATE June 2003 | 3. REPORT TYPE AND DATES COVERED Technical Memorandum | |
| 4. TITLE AND SUBTITLE Advanced Durability and Damage Tolerance Design and Analysis Methods for Composite Structures—Lessons Learned From NASA Technology Development Programs | | 5. FUNDING NUMBERS 706-85-12-01-00 | |
| 6. AUTHOR(S) Charles E. Harris, James H Starnes, Jr., and Mark J. Shuart | | | |
| 7. PERFORMING ORGANIZATION NAME(S) AND ADDRESS(ES) NASA Langley Research Center Hampton, VA 23681-2199 | | 8. PERFORMING ORGANIZATION REPORT NUMBER L-18297 | |
| 9. SPONSORING/MONITORING AGENCY NAME(S) AND ADDRESS(ES) National Aeronautics and Space Administration Washington, DC 20546-0001 | | 10. SPONSORING/MONITORING AGENCY REPORT NUMBER NASA/TM-2003-212420 | |
| 11. SUPPLEMENTARY NOTES An electronic version can be found at http://techreport.larc.nasa.gov/ltrs/ or http://ntrs.nasa.gov . | | | |
| 12a. DISTRIBUTION/AVAILABILITY STATEMENT Unclassified-Unlimited Subject Category 24 Distribution: Standard Availability: NASA CASI (301) 621-0390 | | 12b. DISTRIBUTION CODE | |
| 13. ABSTRACT (Maximum 200 words) Aerospace vehicles are designed to be durable and damage tolerant. Durability is largely an economic life-cycle design consideration whereas damage tolerance directly addresses the structural airworthiness (safety) of the vehicle. However, both durability and damage tolerance design methodologies must address the deleterious effects of changes in material properties and the initiation and growth of microstructural damage that may occur during the service lifetime of the vehicle. Durability and damage tolerance design and certification requirements are addressed for commercial transport aircraft and NASA manned spacecraft systems. The state-of-the-art in advanced design and analysis methods is illustrated by discussing the results of several recently completed NASA technology development programs. These programs include the NASA Advanced Subsonic Technology Program demonstrating technologies for large transport aircraft and the X-33 hypersonic test vehicle demonstrating technologies for a single-stage-to-orbit space launch vehicle. | | | |
| 14. SUBJECT TERMS durability, damage tolerance, fatigue, fracture, structural integrity, structure composite materials, graphite/epoxy, aerospace vehicles | | 15. NUMBER OF PAGES 36 | 16. PRICE CODE |
| 17. SECURITY CLASSIFICATION OF REPORT Unclassified | 18. SECURITY CLASSIFICATION OF THIS PAGE Unclassified | 19. SECURITY CLASSIFICATION OF ABSTRACT Unclassified | 20. LIMITATION OF ABSTRACT UL |